On the Multiscale Formulation and the Derivation of Phase-Change Moving Interfaces

I. L. Ferreira[1] · A. Garcia[2] · A. L. S. Moreira[1]

Abstract

A closed-form analytical solution for transient solidification of multicomponent alloys is proposed by analytically solving the microscale solidification to feed the local conditions, such as surface energy, surface tension, nucleation radius, interface temperature, and solute concentration, necessary to the evolution of macroscopic solidus, liquidus, and eutectic interfaces. Expressions for the critical radius, total free energy, and nucleation rate are derived for homogeneous and heterogeneous nucleation based on recent propositions for nucleation and surface energy. A general solution for interface evolution is proposed, encompassing local temperature and concentration conditions to provide the proper integration of the macroscopic temperature necessary for latent heat release in the solid–liquid phase.

1 Introduction

Solidification plays a vital role in obtaining homogeneous materials and in controlling the structure of castings and ingots in some industrial processes such as continuous casting, surface remelting, casting and laser welding. Therefore, the study

✉ I. L. Ferreira
ileao@ufpa.br

A. Garcia
amaurig@fem.unicamp.br

A. L. S. Moreira
alsm@ufpa.br

[1] Faculty of Mechanical Engineering, Federal University of Pará, UFPA, Augusto Corrêa Avenue 1, Belém, PA 66075-110, Brazil

[2] Department of Manufacturing and Materials Engineering, University of Campinas – UNICAMP, Campinas, SP 13083-860, Brazil

of the solidification of metals has assumed considerable proportions in recent decades since essentially all metals undergo liquid–solid transformation at some stage. In many cases, peculiarities of grain structure, composition and phase distribution result from solidification and these seriously influence subsequent treatments and properties. In this sense, interest in solidification has gone beyond the field of materials and metallurgical engineering, advancing to other applied sciences, in which the knowledge of solidification theory aggregated to the fundamentals of electronics, mechanics, chemistry, physics, applied mathematics, etc., has been used to solve concrete technological problems [1]. Thus, it is essential to understand the underlying mechanisms involved in solidification to control the composition and structure of the solidified metal. Nevertheless, it must be noted that in many cases complete details of the physical mechanisms related to the formation of various types of micro- and macrostructures in the obtained solids are not yet known.

On the other hand, it has been reported that the phenomenon of heat conduction with phase change due to melting–freezing occurs in many areas of current practical interest; however, as the space domain where the heat conduction equation is to be solved changes with time, these are known as moving boundary or Stefan problems [2–4]. Consequently, the mathematical treatment of this problem is complicated since it leads to differential equations presenting nonlinear boundary conditions at the moving interface. Nevertheless, numerous mathematical approaches have been developed to provide an adequate theoretical background for modeling the solidification of metals over the years. In this sense, many mathematical studies aimed to find exact solutions for simple geometries (slabs, cylinders and spheres) or simplified quasi-stationary assumptions that are not realistic in many situations. The analytical methods [1, 2, 5–18], proposed to investigate the solidification process, mainly consider systems with plane geometry due to the greater simplicity of the mathematical treatment as a function of their geometric characteristics. Thus, they present considerable limitations from the point of view of their practical application. It is worth remembering that exact analytical solutions for cylindrical and spherical geometries have not yet been obtained since these geometries present greater mathematical complexity arising from both the mathematical equations and the assumed boundary conditions. The accuracy of numerical solutions [19–42] is often extremely high; however, the use of such solutions requires either programming knowledge and/or special software since these methods demonstrate a certain complexity. They generally lead to a greater proximity of practical cases in industry allowing more real boundary conditions to be assumed for which it would not be possible to obtain analytical solutions. Finally, a number of experimental methods [43–62] have also been used to investigate solidification. Although the several variables and transient conditions involved in the liquid–solid phase change make these methods very specific, they assume an important characteristic because in many cases they are employed to validate analytical and numerical methods.

The main purpose of the present study is to derive an analytical solution for the transient solidification of multicomponent alloys in a slab and deduce a general

form for moving solidus, liquidus, and eutectic interfaces according to the heat flux direction. To achieve this goal, a solution for transient solidification of multicomponent alloys is proposed analytically for microscale solidification to furnish the local conditions necessary for the evolution and proper integration of heat at macroscopic interfaces. New formulations are derived for homogeneous and heterogeneous nucleation based on recent propositions for nucleation and surface energy [17]. A solution for transformation interface evolution is proposed to provide the proper integration of macroscopic latent heat release during the fusion/solidification of multicomponent alloys. Liquidus and eutectic macroscopic interface equations were proposed, and a new derivation was carried out of a well-known analytical transient solution for the solidification of binary alloys [1]. Simulations were performed for different Cu contents and levels of superheat.

2 Mathematical Simplifying Hypotheses

The mathematical simplifying hypotheses assumed in this work can be found in the literature [1, 2]. The purpose of the solution to be obtained is to investigate the solidification of a semi-infinite slab [3, 4]. Thus, the following assumptions are taken into account in this study:

a. The microscopic and macroscopic domains are three-dimensional;
b. The macroscopic domain consists of a solid mould and three metal subdomains: solid, solid and liquid, and liquid;
c. Solidification occurs in a temperature range between solidus and liquidus isotherms, where the latent heat is released;
d. The macroscopic solidification is unidirectional along the *x*-axis, and all limiting wall boundary conditions in both the *y* and *z* axes are assumed to be adiabatic;
e. The microscopic solidification is three-dimensional and the boundary conditions are periodic;
f. The investigated systems are isotropic;
g. The thermal contact resistance at the metal/mould interface is considered;
h. The convection in the melt is neglected;
i. The thermophysical properties are constant within each phase but different among phases.

2.1 Binary Alloy Solidification

Alloys solidify in a temperature range, i.e., an example is between the liquidus and solidus isotherms, in such a way that these boundary conditions can be seen in Fig. 1, demonstrating the temperature profile during unidirectional solidification of a volume element.
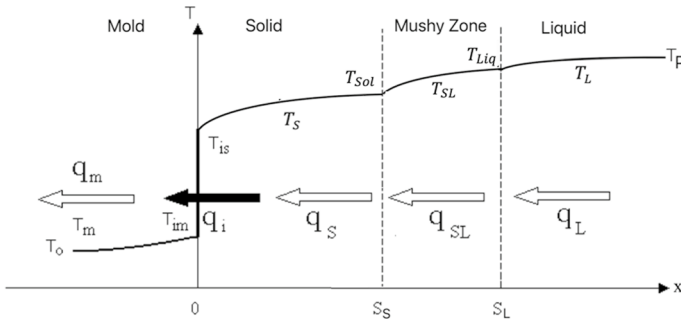
Fig. 1 Temperature as a function of the distance of a volume element during the unidirectional solidification of a binary alloy

where S_S and S_L are the positions of the solidus and liquidus interfaces, respectively, q_L is the heat flux in the liquid phase, q_{SL} is the heat flux in the solid–liquid mixture phase, q_S is the heat flux in the solid phase, q_i is the metal/mould heat flux, q_m is the heat flux in the mould, T_0 is the environmental temperature far from the mould external surface, T_{im} is the mould temperature at the metal/mould interface, T_{is} is the solid temperature at the metal/mould interface, T_S is the temperature of the solid phase, T_{SL} is the temperature of the solid–liquid (mushy zone) phase, T_L is the temperature of the liquid phase and, finally, T_P is the pouring temperature.

Before diving into the problem of the solidification of an alloy, a physical formulation of the solidus and liquidus moving phase-change interfaces must be derived, as far as alloys solidify according to a solidification range, i.e., the latent heat ΔH from a primary α-phase will be released in the temperature range between the liquidus and solidus isotherms, which move at different speeds. Let us consider the heat balance according to Fig. 2.

Recently, Ferreira [17] derived an equation for nucleation based on the thermal field gradient normal to the forming nucleus surface area. This equation is a general form of the Gibbs–Thomson equation, and it is the so-called Gibbs–Thomson-Ferreira equation—GTF [63, 64], which considers the surface stress tensor, the surface energy, and the transformation entropy associated with the normal thermal gradient to a given
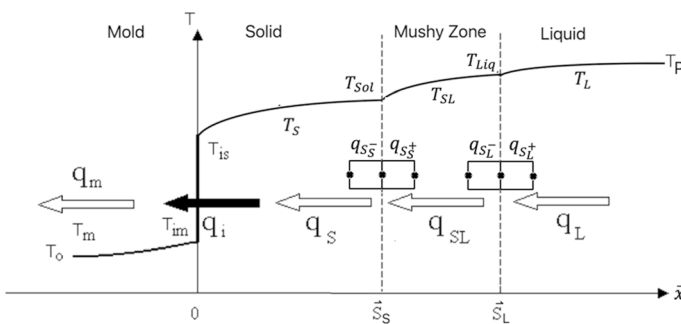

Fig. 2 Temperature distribution as a function of distance in a volume element during unidirectional solidification of a binary alloy

nucleating phase surface area. The application of the GTF equation to phase growth implies in the derivation of a general formulation to deal with the evolution of microscopic transformation interfaces and its application to bridge microscopic to macroscopic phase-change interfaces during transient alloy solidification, which straightaway implies in a multiscale formulation. As an example of multiscale calculation, Karma et al. coupled an atomistic model and Phase-Field for micro and mesoscale solidification simulation [65]. Multiscale formulations can be found in the literature applied to numerical and analytical solidification models [66, 67]. Let us assume a stable nucleus of radius $r \leq r_{Eq}$ for given temperature, volume, pressure and composition gradients, assuming the equilibrium radius r_{Eq} corresponding to the level of surface energy associated only with creating a surface area A_0. The equation expressing the Gibbs–Thomson coefficient for any thermal field gradient for nucleation can be expressed as,

$$\Gamma(\vec{r}) = \nabla \mathbf{T} \cdot \hat{n} A(\vec{r}) \tag{1}$$

where Γ is the Gibbs–Thomson coefficient, $\vec{r}$ is the vector radius, $\nabla \mathbf{T}$ is the thermal field gradient normal to the surface area $A(\vec{r})$, which can be dependent on temperature, volume, pressure and composition gradients, and $\hat{n}$ is the unit normal vector. Gibbs–Thomson coefficient $\Gamma(\vec{r})$ is defined by Ferreira [17] as the thermal field gradient $\nabla \mathbf{T}$ normal to a surface area created in equilibrium A_0, and created and deformed $A(\vec{r})$ in nonequilibrium.

2.2 Application of GTF to the Energy Balances of Liquidus and Solidus Isothermal Surfaces in a Microscopic Domain

To analyze the correct dimensional form for the proposed moving transformation interface formulation, first a heat balance for each transformation interface evolution must be derived, and the relationship between heat flux and latent heat release due to interface coalescence must be established by introducing both properties in Eq. 1. A simple relationship between thermal conductivity κ $\left[\mathrm{W} \cdot \mathrm{m}^{-1} \cdot \mathrm{K}^{-1} \right]$ and molar specific heat capacity c_{vm} $\left[\mathrm{J} \cdot \mathrm{mol}^{-1} \cdot \mathrm{K}^{-1} \right]$ at a given temperature T, demands c_{vm}/v, where v is the phase molar volume $\left[\mathrm{m}^3 \cdot \mathrm{mol}^{-1} \right]$.

Now, considering the solid/liquid transformation, latent heat of solidification, by considering the heat flux of the moving liquidus isotherm at both sides, for $\vec{r} = \vec{S}_L$, $\vec{q}_{SL} = -\vec{k}_{SL} \cdot \nabla \mathbf{T}|_{\vec{r}=\vec{S}_L^-}$ and, $\vec{q}_L = -\vec{k}_L \cdot \nabla \mathbf{T}|_{\vec{r}=\vec{S}_L^+}$, the latent heat of the primary phase, ΔH at $T = T_L$, and Gibbs–Thomson coefficient $\Gamma_L(\vec{S}_L)$, and a heat source q_L similar to what is found in Crank [68],

$$\left\{ \delta \frac{\Delta H}{v_L - v_S} + (1 - \delta) \frac{h_L}{T_L} \frac{\Gamma_L(\vec{r} = \vec{S}_L)}{v_L} \right\} \frac{dA_L}{dt} = \left[\vec{q}_L - \vec{q}_{SL} + \vec{q}(T_L, A_L, t) \right] \cdot \hat{n}_L A_L(\vec{r}) \tag{2a}$$

where δ is the piecewise Heaviside function, which depends on the heat flux signal,

$$\delta(\vec{q}) = \begin{cases} 1 & \text{for } \vec{q} > 0 \\ 0 & \text{for } \vec{q} < 0 \end{cases}$$

If no heat source is present, $\vec{q} = 0$,

$$\left\{ \delta \frac{\Delta H}{v_L - v_S} + (1 - \delta) \frac{h_L}{T_L} \frac{\Gamma_L(\vec{r} = \vec{S}_L)}{v_L} \right\} \frac{dA_L}{dt} = (\vec{q}_L - \vec{q}_{SL}) \cdot \hat{n}_L A_L(\vec{r}) \tag{3}$$

for $\vec{r} = \vec{S}_S$, $\vec{q}_S = -\vec{k}_S \cdot \nabla \mathbf{T}\big|_{\vec{r}=\vec{S}_S^-}$ and $\vec{q}_{SL} = -\vec{k}_{SL} \cdot \nabla \mathbf{T}\big|_{\vec{r}=\vec{S}_S^+}$, the latent heat of the primary phase, ΔH at $T = T_S$, and the Gibbs–Thomson coefficient $\Gamma_S(\vec{S}_S)$,

$$\left\{ \delta \frac{h_S}{T_S} \frac{\Gamma_S(\vec{r} = \vec{S}_S)}{v_S} + (1 - \delta) \frac{\Delta H}{v_L - v_S} \right\} \frac{dA_S}{dt} = \left[\vec{q}_{SL} - \vec{q}_S + \vec{q}(T_S, A_S, t) \right] \cdot \hat{n}_S A_S(\vec{r}) \tag{4}$$

By considering no heat source $\vec{q} = 0$, it gives

$$\left\{ \delta \frac{h_S}{T_S} \frac{\Gamma_S(\vec{r} = \vec{S}_S)}{v_S} + (1 - \delta) \frac{\Delta H}{v_L - v_S} \right\} \frac{dA_S}{dt} = (\vec{q}_{SL} - \vec{q}_S) \cdot \hat{n}_S A_S(\vec{r}) \tag{5}$$

By substituting the thermal gradients and the proper heat fluxes into Eqs. 1–5 allows the determination of the time evolution of the liquidus, Eq. 6 and solidus fronts, Eq. 7. For the liquidus isotherm,

$$\left\{ \delta \frac{\Delta H}{v_L - v_S} + (1 - \delta) \frac{h_L}{T_L} \frac{\Gamma_L(\vec{r} = \vec{S}_L)}{v_L} \right\} \frac{dA_L}{dt} = \left(\vec{k}_{SL} \cdot \nabla \mathbf{T}\big|_{\vec{r}=\vec{S}_L^-} - \vec{k}_L \cdot \nabla \mathbf{T}\big|_{\vec{r}=\vec{S}_L^+} \right) \cdot \hat{n}_L A_L(\vec{r}) \tag{6}$$

and, for the solidus isotherm,

$$\left\{ \delta \frac{h_S}{T_S} \frac{\Gamma_S(\vec{r} = \vec{S}_S)}{v_S} + (1 - \delta) \frac{\Delta H}{v_L - v_S} \right\} \frac{dA_S}{dt} = \left(\vec{k}_S \cdot \nabla \mathbf{T}\big|_{\vec{r}=\vec{S}_S^-} - \vec{k}_{SL} \cdot \nabla \mathbf{T}\big|_{\vec{r}=\vec{S}_S^+} \right) \cdot \hat{n}_S A_S(\vec{r}) \tag{7}$$

The relationship between the Gibbs–Thomson coefficient, $\Gamma_L(\vec{S}_L(\vec{r}))$, and the vector radius, $\vec{r}$, is defined in terms of the surface energy, γ, and the surface stress tensor, $s_{\alpha\beta}$, to consider surface area creation and deformation [17, 69–72], volume ∇V, pressure ∇P, species ∇C_i and temperature ∇T gradients. It is important to mention, that in the case of non-diffusional solid-state phase change, as the martensitic transformation, the term $\frac{dA_S}{dt}$

can be as higher as the Debye speed of sound in the solid [17]. Ferreira proposed a solution for the dependence of the surface energy of the vector radius $\vec{r}(\theta, \phi)$ [17, 73],

$$\Gamma(\vec{r}) = \frac{\gamma\left(\frac{|\vec{r}(\theta,\phi)|}{r_{Eq}}\right)}{\Delta S_V} = \frac{\frac{\gamma_0}{\left(\frac{|\vec{r}(\theta,\phi)|}{r_{Eq}}\right)^2} - s(\vec{r})}{\Delta S_V} \tag{8}$$

where $\vec{r}(\theta, \phi)$ is the radius vector of a variable radius sphere [73], r_{Eq} is the nucleation radius when the surface energy γ_0 is only due to surface area creation A_0, and s is the surface stress tensor, which is written for anisotropic materials [69–72] as

$$s_{\alpha\beta} = \gamma\delta_{\alpha\beta} + \frac{\partial\gamma}{\partial\varepsilon_{\alpha\beta}} \tag{9}$$

For isotropic materials, assuming isothermal volumetric work [71] and isotropic surface stress tensor [70],

$$sA_0\varepsilon = \gamma(\varepsilon)A(\varepsilon) - \gamma_0 A_0 \tag{10}$$

where ε is the strain, $\gamma(\varepsilon)$ is the surface energy due to surface area deformation $A(\varepsilon)$ and s is the isotropic surface stress tensor [69, 71].

The absence of a term to account for the decreasing crystal ordering by increasing crystal defects as a function of the level of undercooling, can culminate, for a given thermal field gradient $\nabla\mathbf{T} = \frac{\partial T}{\partial V}\cdot\nabla V + \frac{\partial T}{\partial \mathbf{P}}\cdot\nabla\mathbf{P} + \sum_{i=1}^{n-1}\frac{\partial T}{\partial C_i}\cdot\nabla C_i + \nabla T$, in a noncrystalline (glassy) material. This dependence of latent heat and transformation entropy on undercooling is well-known and it is based on experimental observations. A suitable equation for the expression of the Gibbs–Thomson first term, Eq. 8, can be derived from homogeneous and heterogeneous nucleation considering the surface energy dependence on surface area creation and deformation [17, 69–72], and both nucleation conditions will provide the same relationship for the critical radius. In the case of homogeneous and heterogeneous nucleation,

$$\Delta G_{\text{Hom}} = -\frac{4}{3}\pi r^3 \Delta H \frac{\Delta T}{T_F} + 4\pi r^2 \gamma_{SL} \tag{11}$$

$$\Delta G_{\text{Het}} = \left(2 - 3\cos\theta + \cos^3\theta\right)\left(-\frac{1}{3}\pi r^3 \Delta H \frac{\Delta T}{T_F} + \pi r^2 \gamma_{SL}\right) \tag{12}$$

By deriving Eqs. 11 and 12 with respect to r at $r = r_C$ gives,

$$\left.\frac{\partial\Delta G_{\text{Hom}}}{\partial r}\right|_{r=r_C} = -4\pi r_C^2 \Delta H \frac{\Delta T}{T_F} + 8\pi r_C \gamma_{SL} + 4\pi r_C^2 \left.\frac{\partial\gamma_{SL}}{\partial r}\right|_{r=r_C} = 0 \tag{13}$$

$$\left.\frac{\partial\Delta G_{\text{Het}}}{\partial r}\right|_{r=r_C} = \left(2 - 3\cos\theta + \cos^3\theta\right)\left(-\pi r_C^2 \Delta H \frac{\Delta T}{T_F} + 2\pi r_C \gamma_{SL} + \pi r_C^2 \left.\frac{\partial\gamma_{SL}}{\partial r}\right|_{r=r_C}\right) = 0 \tag{14}$$

The critical radii for nonequilibrium homogeneous and heterogeneous nucleation are the same and given by,

$$r_C = \frac{2\gamma_{SL}}{\Delta H \frac{\Delta T}{T_F} - \frac{\partial \gamma_{SL}}{\partial r}\Big|_{r=r_C}} = \frac{2}{\Delta T} \frac{\gamma_{SL}}{\left(\Delta S - \frac{1}{\Delta T}\frac{\partial \gamma_{SL}}{\partial r}\Big|_{r=r_C}\right)} = \frac{2}{\Delta T}\frac{\gamma_{SL}}{\left(\Delta S - \Delta S_{surf}\right)} = \frac{2}{\Delta T}\Gamma$$

(15)

On the other hand, a more suitable form to express the Gibbs–Thomson coefficient for nonequilibrium nucleation to be applied to Eqs. 1, and 7 can be deduced from Eq. 15 as follows

$$\Gamma = \frac{\gamma_{SL}}{\frac{\Delta H}{T_F} - \frac{1}{\Delta T}\frac{\partial \gamma_{SL}}{\partial r}\Big|_{r=r_C}} = \frac{\gamma_{SL}}{\Delta S - \Delta S_{Surf}}$$

(16)

and, the latent heat release is defined as $\Delta H^* = \Delta H - \frac{\partial \gamma_{SL}}{\partial r}$. By comparing it to equilibrium nucleation, in which the surface energy γ_0 considers only the surface area creation A_0,

$$r_C^{Eq} = \frac{2\gamma_0}{\Delta H \frac{\Delta T}{T_F}} = \frac{2\gamma_0}{\Delta S_V \Delta T} = \frac{2}{\Delta T}\Gamma^{Eq}$$

(17)

The results of Eqs. 13 and 14 confirms that crystallinity is dependent on the degree of undercooling ΔT and on the variation in surface energy with respect to the nucleation radius $\frac{\partial \gamma_{SL}}{\partial r}\Big|_{r=r_C}$, which defines the surface entropy, $\Delta S_{surf} = \frac{1}{\Delta T}\frac{\partial \gamma_{SL}}{\partial r}\Big|_{r=r_C}$. Once the surface energy is a function of temperature, concentration, volume and pressure gradients according to Eq. 1 [17], the condition for liquid–solid or solid–solid transformation for nonregular crystals, Eq. 16, considering an undercooled liquid can be expressed as

$$\frac{\Delta H}{T_F} < \frac{1}{\Delta T}\frac{\partial \gamma_{SL}}{\partial r}\Big|_{r=r_C}$$

(18)

Similar to a superheated phase nucleation,

$$\frac{\Delta H}{T_F} > \frac{1}{\Delta T}\frac{\partial \gamma_{SL}}{\partial r}\Big|_{r=r_C}$$

(19)

By expressing in terms of entropy, for an undercooled phase,

$$\Delta S_V < \Delta S_{surf}$$

(20)

For a superheated phase nucleation,

$$\Delta S_V > \Delta S_{surf}$$

(21)

For a regular monocrystal,

$$\Delta S_{Surf} = \frac{1}{\Delta T} \left. \frac{\partial \gamma_{SL}}{\partial r} \right|_{r=r_C} = 0 \tag{22}$$

By combining Eqs. 1 and 16 gives

$$\Gamma(\vec{r}) = \frac{\gamma_{SL}}{\Delta S - \frac{1}{\Delta T} \frac{\partial \gamma_{SL}}{\partial \vec{r}} \Big|_{\vec{r}=\vec{r}_C}} = \nabla \mathbf{T} \cdot \hat{n} A(\vec{r}) = \left[\frac{\partial T}{\partial V} \cdot \nabla V + \frac{\partial T}{\partial \mathbf{P}} \cdot \nabla \mathbf{P} + \sum_{i=1}^{n-1} \frac{\partial T}{\partial C_i} \cdot \nabla C_i + \nabla T \right] \cdot \hat{n} A(\vec{r}) \tag{23}$$

By substituting the critical radius from Eqs. 15 into 11 and Eq. 12, nonequilibrium critical free energy equations are obtained for homogeneous $\Delta G_{C,Hom}$, and heterogeneous $\Delta G_{C,Het}$ nucleation, given by,

$$\Delta G_{C,Hom} = \frac{16}{3} \pi \frac{\gamma_{SL}^3 \left(\Delta S - \frac{3}{\Delta T} \frac{\partial \gamma_{SL}}{\partial r} \right)}{\Delta T^2 \left(\Delta S - \frac{1}{\Delta T} \frac{\partial \gamma_{SL}}{\partial r} \right)^3} \tag{24}$$

and,

$$\Delta G_{C,Het} = \frac{16}{3} \pi \frac{\gamma_{SL}^3 \left(\Delta S - \frac{3}{\Delta T} \frac{\partial \gamma_{SL}}{\partial r} \right)}{\Delta T^2 \left(\Delta S - \frac{1}{\Delta T} \frac{\partial \gamma_{SL}}{\partial r} \right)^3} \left[\frac{1}{4} \left(2 - 3\cos\theta + \cos^3\theta \right) \right] \tag{25}$$

The nucleation rate for homogeneous and heterogeneous nucleation can be expressed as

$$I_{Hom} = \left(\frac{D_L}{a^2} \right) \left(\frac{4\pi r_C^2}{a^2} \right) C_L \exp \left[-\frac{16}{3} \pi \frac{\gamma_{SL}^3 \left(\Delta S - \frac{3}{\Delta T} \frac{\partial \gamma_{SL}}{\partial r} \right)}{\Delta T^2 \left(\Delta S - \frac{1}{\Delta T} \frac{\partial \gamma_{SL}}{\partial r} \right)^2 k_B T} \right] \tag{26}$$

and, for heterogeneous nucleation

$$I_{Het} = \left(\frac{D_L}{a^2} \right) \left[\frac{2\pi r_C^2 (1 - \cos\theta)}{a^2} \right] C_a \exp \left\{ -\frac{16}{3} \pi \frac{\gamma_{SL}^3 \left(\Delta S - \frac{3}{\Delta T} \frac{\partial \gamma_{SL}}{\partial r} \right)}{\Delta T^2 \left(\Delta S - \frac{1}{\Delta T} \frac{\partial \gamma_{SL}}{\partial r} \right)^3 k_B T} \left[\frac{1}{4} \left(2 - 3\cos\theta + \cos^3\theta \right) \right] \right\} \tag{27}$$

Equation 8 can be rewritten in terms of Eq. 23 to incorporate the surface entropy $\Delta S_{Surf} = \frac{1}{\Delta T} \left. \frac{\partial \gamma_{SL}}{\partial \vec{r}} \right|_{\vec{r}=\vec{r}_C}$ by considering a solution for surface energy in terms of a variable radius sphere,
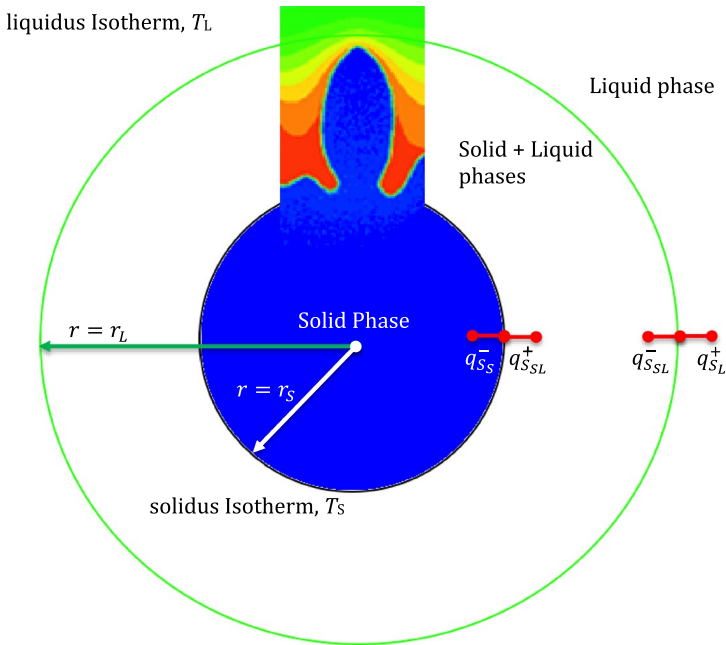
Fig. 3 Schematic representation of an alloy solidification range in the microscopic domain

$$
\Gamma(\vec{r}) = \frac{\gamma\left(\frac{|\vec{r}(\theta,\phi)|}{r_{Eq}}\right)}{\Delta S_V - \frac{1}{\Delta T}\frac{\partial \gamma_{SL}}{\partial \vec{r}}\Big|_{\vec{r}=\vec{r}_C}} = \frac{\frac{\gamma_0}{\left(\frac{|\vec{r}(\theta,\phi)|}{r_{Eq}}\right)^2} - s(\vec{r})}{\Delta S_V - \frac{1}{\Delta T}\frac{\partial \gamma_{SL}}{\partial \vec{r}}\Big|_{\vec{r}=\vec{r}_C}} = \nabla \mathbf{T} \cdot \hat{n} A(\vec{r})
$$

$$
= \left[\frac{\partial T}{\partial V}\cdot\nabla V + \frac{\partial T}{\partial \mathbf{P}}\cdot\nabla\mathbf{P} + \sum_{i=1}^{n-1}\frac{\partial T}{\partial C_i}\cdot\nabla C_i + \nabla T\right]\cdot\hat{n}A(\vec{r})
$$

(28)

A stable nucleus shape is not assumed to be a regular sphere, because it is only a special case, $|\vec{r}| = r_0$ [17], but its shape depends on the thermal field gradient pattern normal to its surface, a function of the azimuth θ and zenith ϕ angles, $\vec{r}(\theta,\phi)$ in $x_{0,i}$, which is better defined in terms of a vector radius $\vec{r}$ that describes a variable radius sphere. Now, the shape of the nucleus can be engineered through the knowledge of the thermal field gradient $\nabla\mathbf{T} = \left[\frac{\partial T}{\partial V}\cdot\nabla V + \frac{\partial T}{\partial \mathbf{P}}\cdot\nabla\mathbf{P} + \sum_{i=1}^{n-1}\frac{\partial T}{\partial C_i}\cdot\nabla C_i + \nabla T\right]$, expressed as a function of volume ∇V, pressure $\nabla\mathbf{P}$, species ∇C_i and temperature ∇T gradients. A set of points in $\mathbb{R}^3$ defines a sphere in Euclidean coordinates in 3-space, with a variable distance $r(\theta,\phi)$, as a function of any property $p \in \mathbb{R}^3$, defined as a vector radius $\vec{r}$ from a set of fixed center points $x_{0,i}$, $r^2(p) = \sum_{i=1}^{3}\left(x_i - x_{0,i}\right)^2$. There are several algorithms applied to sphere decoding—SD. One situation can be posed as a known surface area, and a set of unknown vector radii must be found as described in Di et al. [73]. In the present formulation, the property $p = \nabla\mathbf{T}$.

Figure 3 shows a schematic domain representation for nucleation and solidification evolution interfaces of an alloy in the microscopic domain $r \in \mathbb{R}^3$, consisting of three distinct subdomains: a solid for $0 < r < S_S$, solid and liquid for $S_S \leq r \leq S_L$, and liquid for $r > S_L$ phases. For the microscopic domain, Eqs. 3, 4, 6, and 7 can be applied directly.

2.3 Application of Energy Balances of Liquidus and Solidus Isothermal Surfaces in the Macroscopic Domain inside a Slab for Unidirectional Solidification

In the present model proposition for the unidirectional transient solidification of multicomponent alloys, the microscopic and macroscopic domains are defined in $\mathbb{R}^3$. Nevertheless, solidification occurs macroscopically only along the x coordinate. The mathematical formulation of transient solidification of a binary alloy inside a slab, consisting of a cross-section $A_0 = Y_0 Z_0$ and height $h = X_o$ along with x coordinates, is derived in terms of macroscopic phase subdomains for the temperature fields inside the solid $T_S(x, t)$, solid and liquid $T_{SL}(x, t)$, and liquid $T_L(x, t)$ phases.

The thermal gradients at each transformation interface are written in terms of the x coordinate for the liquidus and solidus (indeed eutectic) moving interfaces and are given in terms of the heat flow direction δ as the follows:

$$\left\{ \delta \frac{\Delta H}{v_L - v_S} + (1 - \delta) \frac{h_L}{T_L} \frac{\Gamma_L\left(\vec{r} = \vec{S}_L\right)}{v_L} \right\} \frac{dA_L}{dt} = \left(k_L \cdot \left. \frac{\partial \mathrm{T}}{\partial \mathrm{x}} \right|_{x=S_L^+} - k_{SL} \cdot \left. \frac{\partial \mathrm{T}}{\partial \mathrm{x}} \right|_{x=S_L^-} + \vec{q}(T_L, A_L, t) \right) \cdot \hat{n}_L A_L$$

(29)

and,

$$\left\{ \delta \frac{h_S}{T_S} \frac{\Gamma_S\left(\vec{r} = \vec{S}_S\right)}{v_S} + (1 - \delta) \frac{\Delta H}{v_L - v_S} \right\} \frac{dA_S}{dt} = \left(k_{SL} \cdot \left. \frac{\partial \mathrm{T}}{\partial \mathrm{x}} \right|_{x=S_S^+} - k_S \cdot \left. \frac{\partial \mathrm{T}}{\partial \mathrm{x}} \right|_{x=S_S^-} + \vec{q}(T_S, A_S, t) \right) \cdot \hat{n}_S A_S$$

(30)

where A is surface area normal to the heat flux, which is independent of the moving surface position, and q_L and q_S are source terms. In the case of $\Gamma_L(\vec{r})$ and $\Gamma_S(\vec{r})$ formulations, such as the Representative Elementary Volume [66] and the Volume Averaged Technique [67], it is necessary to capture the mean radius from the microscopic domain.

2.4 Mathematical Model Physical Assumptions

As proposed by Garcia and Prates for solidification of metals in cooled moulds [6] and by Garcia, Clyne and Prates in massive moulds [7], a virtual system can be introduced in which heat flow is treated in two regimes, as shown in Fig. 4 for a binary alloy in a massive mould [11]. In the virtual system, the metal/mould heat transfer coefficient is represented by two parcels of pre-existing adjuncts of
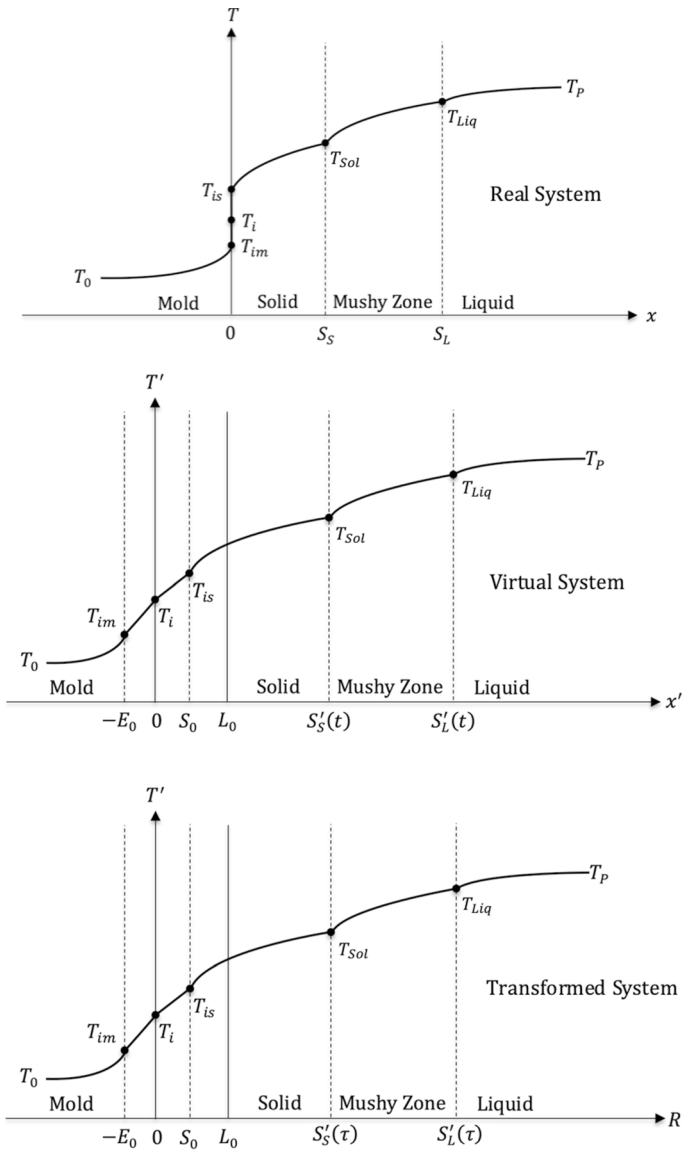
Fig. 4 Temperature (T)-distance (x) profiles during solidification in the real, virtual and transformed virtual systems

material: a solid layer of metal (S_0), a layer of metal due to the solid and mushy zone (L_0), and, finally, an existing layer of mould (E_0).

In the virtual system, Eq. 1 is exactly applicable and heat flow in the metal and mould are connected by a hypothetical plane of invariant temperature Ti. The transposition of variables between real and virtual systems is given by the following expressions:

$$x^{'} = x + L_0, \text{for} x > 0 \tag{31}$$

$$x^{'} = x - E_0, \text{for} x < 0 \tag{32}$$

$$S_S^{'} = S_S + S_0 \tag{33}$$

$$S_L^{'} = S_L + L_0 \tag{34}$$

$$t_S^{'} = t_S + t_{0S} \tag{35a}$$

$$t_L^{'} = t_L + t_{0L} \tag{35b}$$

By considering t_0 as the solidification time of a virtual thickness S_0 as found in [11], the time is assumed to be

$$t^{'} = t + t_0 \tag{36}$$

where x and $x^{'}$ represent the distances from the metal/mould interface, S_S and $S_S^{'}$ are the solidus isotherm interface in real and virtual systems, S_L and $S_L^{'}$ are the liquidus interface isotherm interface in real and virtual systems, and t/t' are the time from zero point in the real and virtual systems, respectively, E_0 is the thickness of mould pre-existing adjunct in the virtual system, S_0 is the thickness of solid pre-existing adjunct in the virtual system, and L_0 is the thickness of mushy and solid pre-existing adjuncts in the virtual system.

For alloy solidification [6, 7, 11], the temperature-distance system is given in Fig. 2. At $x = S_L$ and $t > 0$, the temperature of the moving boundary is $T = T_L$ after a time δ, and the solidus isotherm moving boundary at $x = S_S$ is $T = T_S$. The boundary conditions are written in terms of the virtual system,

$$\frac{\partial T}{\partial t'} = a_m \left(\frac{P}{x'} \frac{\partial T}{\partial x'} + \frac{\partial^2 T}{\partial x'^2} \right) - E_0 < x^{'} < L_0 \text{ and } t > 0 \tag{37}$$

$$\frac{\partial T}{\partial t'} = a_s \left(\frac{P}{x'} \frac{\partial T}{\partial x'} + \frac{\partial^2 T}{\partial x'^2} \right) L_0 < x^{'} < S_S^{'} \text{ and } t > 0 \tag{38}$$

$$\frac{\partial T}{\partial t'} = a_{sl} \left(\frac{P}{x'} \frac{\partial T}{\partial x'} + \frac{\partial^2 T}{\partial x'^2} \right) S_S^{'} < x^{'} < S_L^{'} \text{ and } t > 0 \tag{39}$$

$$\frac{\partial T}{\partial t'} = a_l \left(\frac{P}{x'} \frac{\partial T}{\partial x'} + \frac{\partial^2 T}{\partial x'^2} \right) S_L^{'} x^{'} < \infty \text{ and } t > 0 \tag{40}$$

for $t^{'} = 0$,

$$0 \leq x' \leq \infty, T = T_0 \tag{41}$$

for $t' > 0$,

$$x' = -\infty, T_m = T_0 \tag{42}$$

$$x' = 0, T_m = T_S = T_i \tag{43}$$

$$x' = S'_S, T_S = T_{Sol} \tag{44}$$

$$x' = S'_S, T_{SL} = T_{Sol} \tag{45}$$

$$x' = S'_L, T_{SL} = T_{Liq} \tag{46}$$

$$x' = S'_L, T_L = T_{Liq} \tag{47}$$

$$x' = +\infty, T_L = T_P \tag{48}$$

$$\left\{ (1-\delta)\frac{\Delta H}{v_L - v_S} + \delta\frac{h_S}{T_S}\frac{\Gamma_S\left(\vec{r} = \vec{S}_S\right)}{v_S} \right\}\frac{dA'_S}{dt'} = \left[k_{SL} \cdot \frac{\partial T}{\partial x'}\bigg|_{x'=S'^+_S} - k_S \cdot \frac{\partial T}{\partial x'}\bigg|_{x'=S'^-_S} \right]A'_S \tag{49}$$

$$\left\{ \delta\frac{\Delta H}{v_L - v_S} + (1-\delta)\frac{h_L}{T_L}\frac{\Gamma_L(r = S_L)}{v_L} \right\}\frac{dA'_L}{dt'} = \left[k_L \cdot \frac{\partial T}{\partial x'}\bigg|_{x'=S'^+_L} - k_{SL} \cdot \frac{\partial T}{\partial x'}\bigg|_{x'=S'^-_L} \right]A'_L \tag{50}$$

where $A'_L = r^2 \int_{\phi=0}^{2\pi}\int_{\theta=0}^{\frac{\pi}{2}}\cos\theta\sin\theta d\theta d\phi$ and $A'_S = r^2 \int_{\phi=0}^{2\pi}\int_{\theta=0}^{\frac{\pi}{2}}\cos\theta\sin\theta d\theta d\phi$ are normal to the surface area independent of the moving surface position. By considering the heat flux direction, $A'_L = \delta 8\pi r + (1-\delta)8(\pi r)^2$, and $dA'_L = 8\pi r dr$. In the case of $A'_S = (1-\delta)8\pi r + \delta 8(\pi r)^2$ and, $dA'_S = 8\pi r dr$. k_S is the solid phase, k_{SL} is the mushy zone and k_L is the liquid phase thermal conductivities. T_0 is the initial temperature of the liquid phase, and Γ_S and Γ_L are the Gibbs–Thomson at the eutectic and liquidus isotherms, respectively.

2.4.1 Solid Region

Applying the performed change of variables to the exact solution based on the error function, which represents the solidification of a semi-infinite slab, gives

$$T_S(x', t') = A_S + B_S erf\left(\frac{x'}{2\sqrt{a_s t'}}\right) \tag{51}$$

Then, applying the boundary conditions of Eqs. 43 into 51, provides

$$A_S = T_i \tag{52}$$

and introducing the similarity variable ϕ_1,

$$\frac{S_S'}{2\sqrt{a_s t'}} = \phi_1 \frac{x'}{S_S'} = \phi_1 \frac{x + L_0}{S_S + L_0} \tag{53}$$

Substituting the boundary conditions of Eqs. 44, 52 and the function argument Eqs. 53 into 51, the integration constant B_S can be derived as

$$B_S = \frac{T_f - T_i}{erf(\phi_1)} \tag{54}$$

Substituting the obtained integration constants Eqs. 52, 54 and the error function argument Eqs. 53 into 51, an expression for the temperature profile in the solid phase is obtained as follows:

$$T_S(x, S_S) = T_i + \frac{T_{Sol} - T_i}{erf(\phi_1)} erf\left(\phi_1 \frac{x + L_0}{S_S + L_0}\right) \tag{55}$$

2.4.2 Liquid Region

The solution for Eq. 40 for the liquid phase, considering the transformed radial variable, can be expressed as

$$T_L(x', t') = A_L + B_L erf\left(\frac{x'}{2\sqrt{a_L t'}}\right) \tag{56}$$

Then, applying the boundary conditions given by Eqs. 4) and Eq. 48 into Eq. 56, provides

$$T_{Liq} = A_L + B_L erf\left(\frac{S_L'}{2\sqrt{a_L t'}}\right) \tag{57}$$

and,

$$T_P = A_L + B_L \tag{58}$$

Then, A_L and B_L are provided as

$$A_L = T_P - \frac{(T_P - T_{Liq})}{1 - erf(n\phi_2)} \tag{59}$$

and,

$$B_L = \frac{\left(T_P - T_{Liq}\right)}{1 - erf\left(n\phi_2\right)} \tag{60}$$

and the similarity variable ϕ_2,

$$\frac{x'}{2\sqrt{a_L t'}} \frac{\sqrt{a_{SL}|_{S'_L^-} t'}}{\sqrt{a_{SL}|_{S'_L^-} t'}} = m\phi_2 \frac{x'}{S'_L} = m\phi_2 \frac{x + L_0}{S_L + L_0} \tag{61}$$

where n is the relation between the solid–liquid (mushy zone) and liquid phase heat diffusivities, given by

$$m = \sqrt{\frac{a_{SL}|_{S'_L^-}}{a_L}} \tag{62a}$$

By solving the mean integral at the neighborhood of S'_L^- for thermal conductivity $k_{SL}|_{S'_L^-}$ and density $d_{SL}|_{S'_L^-}$,

$$k_{SL}|_{S'_L^-} = \frac{\left[k_S\left(G_L - \frac{G_L^2}{2}\right) + k_L\frac{G_L^2}{2}\right]_{g_{Lmin}}^{g_{Lmax}}}{\left(g_{Lmax} - g_{Lmin}\right)} \cong \frac{\left[k_S\left(G_L - \frac{G_L^2}{2}\right) + k_L\frac{G_L^2}{2}\right]_{0.99}^{1.00}}{1.00 - 0.99} \tag{62b}$$

and,

$$d_{SL}|_{S'_L^-} = \frac{\left[d_S\left(G_L - \frac{G_L^2}{2}\right) + k_L\frac{G_L^2}{2}\right]_{g_{Lmin}}^{g_{Lmax}}}{\left(g_{Lmax} - g_{Lmin}\right)} \cong \frac{\left[d_S\left(G_L - \frac{G_L^2}{2}\right) + d_L\frac{G_L^2}{2}\right]_{0.99}^{1.00}}{1.00 - 0.99} \tag{62c}$$

Finally,

$$c_{PSL}|_{S'_L^-} = c_{PL} + \frac{\Delta H}{T_L} \tag{62d}$$

Then, the thermal diffusivity in the neighborhood of S'_L^- can be expressed as

$$a_{SL}|_{S'_L^-} = \frac{k_{SL}|_{S'_L^-}}{d_{SL}|_{S'_L^-} c_{PSL}|_{S'_L^-}} \tag{62e}$$

For comparison purposes with Garcia's model [1],

$$c_{PSL}|_{S'_L^-} = c_{PSL}|_{S'_L^+} = c_{PL} + \frac{\Delta H}{T_L - T_E} \tag{62f}$$

Substituting the obtained integration constants, Eqs. 59–62 into Eq. 56 provides an expression for the liquid temperature profile,

$$T_L\left(x, S_L\right) = T_P + \frac{T_P - T_{Liq}}{1 - erf\left(m\phi_2\right)}\left[1 - erf\left(m\phi_2\frac{x + L_0}{S_L + L_0}\right)\right] \tag{63}$$

2.4.3 Mold Region

The solution of Eq. 37 for the mould region can be expressed as

$$T_m\left(x', t'\right) = A_m + B_m erf\left(\frac{x'}{2\sqrt{a_m t'}}\right) \tag{64}$$

Then, applying the boundary conditions of Eqs. 42 into 64, provides

$$T_m\left(-\infty, t'\right) = T_0 = A_m - B_m \tag{65}$$

By applying boundary conditions Eqs. 43 into 64, gives

$$A_m = T_i \tag{66}$$

where

$$B_m = T_i - T_0 \tag{67}$$

and, introducing the geometric correlation Θ into the similarity variable Λ,

$$\frac{x'}{2\sqrt{a_m t'}} = \sqrt{\frac{a_s}{a_m}}\phi_1\frac{x'}{S_S'} = N\phi_1\frac{x'}{S_S'} = N\phi_1\frac{x - E_0}{S_S + L_0} \tag{68}$$

where n is the relationship between the heat diffusivities of the solid and liquid phases, given by

$$N = \sqrt{\frac{a_S}{a_m}} = \sqrt{\frac{k_S c_m d_m}{k_m c_S d_S}} \tag{69}$$

Substituting the boundary conditions of Eqs. 66, 67 and 58 into Eq. 64, provides an expression for the temperature profile in the mould:

$$T_m\left(x, S_S\right) = T_i + \left(T_0 - T_i\right)erf\left(N\phi_1\frac{x - E_0}{S_S + L_0}\right) \tag{70}$$

2.4.4 Determination of the Equilibrium Temperature at the Metal/Mould Interface (T_i)

The equilibrium temperature at the metal/mould interface can be derived by determining the heat balance at this interface,

$$q_m\big|_{x'=-0} = q_S\big|_{x'=+0} \tag{71}$$

which provides

$$k_m\left(\frac{\partial T_m}{\partial x'}\right)\bigg|_{x'=-0} = k_S\left(\frac{\partial T_S}{\partial x'}\right)\bigg|_{x'=+0} \tag{72}$$

The derivatives of Eqs. 55 and 70, with respect to x' give, respectively

$$\left(\frac{\partial T_S}{\partial x'}\right)\bigg|_{x'=+0} = \frac{2}{\sqrt{\pi}}\frac{(T_{Sol}-T_i)}{erf(\phi_1)}\phi_1\frac{1}{S_S'} \tag{73}$$

and,

$$\left(\frac{\partial T_m}{\partial x'}\right)\bigg|_{x'=+0} = \frac{2}{\sqrt{\pi}}N(T_i-T_0)\phi_1\frac{1}{S_S'} \tag{74}$$

By substituting Eqs. 73 and 74 into Eq. 72

$$T_i = T_0 + (T_{Sol}-T_0)\frac{M}{M+erf(\phi_1)} \tag{75}$$

where M is defined as

$$\frac{k_m}{k_S}N = \frac{k_m}{k_S}\sqrt{\frac{k_S C_{pm}\rho_m}{k_m C_{pS}\rho_S}} = \frac{1}{M} \tag{76}$$

and, Eq. 55 for the solid region

$$T_S(x,S_S) = T_0 + \frac{T_{Sol}-T_0}{M+erf(\phi_1)}\left[M+erf\left(\phi_1\frac{x+S_0}{S_S+L_0}\right)\right] \tag{77}$$

Substituting T_i from Eq. 75 into Eq. 70 mould temperature profile,

$$T_m(x,S_S) = T_0 + \frac{M(T_{Sol}-T_0)}{M+erf(\phi_1)}\left\{1+erf\left[N\phi_1\left(\frac{x-E_0}{S_S+L_0}\right)\right]\right\} \tag{78}$$

2.4.5 Solid + Liquid Region

The solution of Eq. (39) for the mushy region can be written as follows:

$$T_{SL}(x',t') = A_{SL} + B_{SL}erf\left(\frac{x'}{2\sqrt{a_{SL}t'}}\right) \tag{79}$$

By applying the boundary conditions Eqs. 45 and 46,

$$T_{Sol} = A_{SL} + B_{SL} erf\left(\frac{S'_S}{2\sqrt{a_{SL}t'}}\right) \tag{80}$$

and,

$$T_{Liq} = A_{SL} + B_{SL} erf\left(\frac{S'_L}{2\sqrt{a_{SL}t'}}\right) \tag{81}$$

A possible relationship between Eqs. 80 and 81 arguments can be made by rearranging in terms of similarity variables ϕ_1 and ϕ_2, and by combining them with Eq. 61

$$\phi_2 = \frac{S'_L}{2\sqrt{a_{SL}\big|_{S'^+_S}t'}} = \frac{S'_L}{2\sqrt{a_S t'}}\frac{\sqrt{a_S}}{\sqrt{a_{SL}\big|_{S'^+_S}}}\frac{S'_S}{S'_S} = n\phi_1\frac{S'_L}{S'_S} \tag{82a}$$

By solving the mean integral at the neighborhood of S'^+_S for thermal conductivity $k_{SL}\big|_{S'^+_S}$ and density $d_{SL}\big|_{S'^+_S}$,

$$k_{SL}\big|_{S'^+_S} = \frac{\left[k_S\left(G_L - \frac{G_L^2}{2}\right) + k_L\frac{G_L^2}{2}\right]_{g_{Lmin}}^{g_{Lmax}}}{(g_{Lmax} - g_{Lmin})} \cong \frac{\left[k_S\left(G_L - \frac{G_L^2}{2}\right) + k_L\frac{G_L^2}{2}\right]_0^{0.01}}{0.01 - 0} \tag{82b}$$

and

$$d_{SL}\big|_{S'^+_S} = \frac{\left[d_S\left(G_L - \frac{G_L^2}{2}\right) + k_L\frac{G_L^2}{2}\right]_{g_{Lmin}}^{g_{Lmax}}}{(g_{Lmax} - g_{Lmin})} \cong \frac{\left[d_S\left(G_L - \frac{G_L^2}{2}\right) + d_L\frac{G_L^2}{2}\right]_0^{0.01}}{0.01 - 0} \tag{82c}$$

Finally,

$$c_{PSL}\big|_{S'^+_S} = c_{PS} + \frac{\Delta H}{T_{Sol}} \tag{82d}$$

Then, the thermal diffusivity in the neighborhood of S'^-_L can be expressed as

$$a_{SL}\big|_{S'^+_S} = \frac{k_{SL}\big|_{S'^+_S}}{d_{SL}\big|_{S'^+_S}c_{PSL}\big|_{S'^+_S}} \tag{82e}$$

where

$$n = \sqrt{\frac{a_S}{a_{SL}\big|_{S'^+_S}}} \tag{83}$$

The present model equivalent to Garcia's model demands c_{PSL} defined as given by Eq. 62f.

Now, integration constants A_{SL} and B_{SL} can be determined as follows:

$$A_{SL} = T_{Liq} - \frac{T_{Liq} - T_{Sol}}{\text{erf}(\phi_2) - \text{erf}(n\phi_1)} erf(\phi_2) \tag{84}$$

and,

$$B_{SL} = \frac{T_{Liq} - T_{Sol}}{\text{erf}(\phi_2) - \text{erf}(n\phi_1)} \tag{85}$$

By combining Eq. 82 with Eqs. 53, 83 provides

$$\frac{x'}{2\sqrt{a_L t'}} = \phi_1 \frac{x'\sqrt{a_S}}{S'_S\sqrt{a_{SL}|_{S'_S^+}}} = n\phi_1 \frac{x'}{S'_S} = \phi_2 \frac{x'}{S'_L} = \phi_2 \frac{x + L_0}{S_L + L_0} \tag{86}$$

The temperature profile for the mushy zone can be written by substituting Eqs. 84, 85 and Eqs. 86 into 79

$$T_{SL}(x', S_L) = T_{Liq} - \frac{T_{Liq} - T_{Sol}}{\text{erf}(\phi_2) - \text{erf}(n\phi_1)} \left\{ erf(\phi_2) - \text{erf}\left[\phi_2\left(\frac{x + L_0}{S_L + L_0}\right)\right]\right\} \tag{87}$$

2.4.6 Determination of Similarity Variables (ϕ_1, ϕ_2)

Regarding the heat balance equation at the moving solid/liquid interface, Eqs. 49 and 50, the derivatives with respect to x' at the interface position S'_S and S'_L of Eqs. 63, 77, and Eq. 87) for liquid, solid and solid–liquid phases, respectively, provide the following equations:

$$\left(\frac{\partial T_L}{\partial x'}\right) = \frac{2}{\sqrt{\pi}} \frac{m\phi_2}{S'_L} \frac{(T_P - T_{Liq})}{1 - erf(m\phi_2)} \exp\left[-\left(m\phi_2 \frac{x'}{S'_L}\right)^2\right] \tag{88}$$

and,

$$\left(\frac{\partial T_S}{\partial x'}\right) = \frac{2}{\sqrt{\pi}} \frac{\phi_1}{S'_S} \frac{(T_{Sol} - T_0)}{M + erf(\phi_1)} \exp\left[-\left(\phi_1 \frac{x'}{S'_S}\right)^2\right] \tag{89}$$

and,

$$\left(\frac{\partial T_{SL}}{\partial x'}\right) = \frac{2}{\sqrt{\pi}} \frac{n\phi_1}{S'_S} \frac{(T_{Liq} - T_{Sol})}{\text{erf}(\phi_2) - erf(n\phi_1)} \exp\left[-\left(n\phi_1 \frac{x'}{S'_S}\right)^2\right] \tag{90}$$

The time derivatives of the expression for the similarity variables for ϕ_1 and ϕ_2 and their derivatives with respect to with x' for S'_L are

$$S'_L = 2\phi_2\sqrt{a_L t'} \tag{91}$$

and,

$$S'_L \frac{dS'_L}{dt'} = 2\phi_2^2 a_L \tag{92}$$

and, for S'_S provides,

$$S'_S = 2\phi_1\sqrt{a_S t'} \tag{93}$$

and,

$$S'_S \frac{dS'_S}{dt'} = 2\phi_1^2 a_S \tag{94}$$

Combined with Eq. 83,

$$\frac{\phi_2}{S'_L} = n\frac{\phi_1}{S'_S} \tag{95}$$

By substituting Eqs. 88–95 into Eq. 49) and Eq. (50), expressions for ϕ_1 and ϕ_2 are obtained:

$$
\sqrt{\pi}\left\{ \delta\frac{\Delta H}{v_L - v_S} + (1-\delta)\frac{h_L}{T_L}\frac{\Gamma_L(r = S_L)}{v_L} \right\}\phi_2 a_L
$$
$$
= \left[k_L\frac{m(T_P - T_{Liq})}{[1 - \mathrm{erf}(m\phi_2)]\exp(m^2\phi_2^2)} - k_{SL}\frac{(T_{Liq} - T_{Sol})}{[\mathrm{erf}(\phi_2) - \mathrm{erf}(n\phi_1)]\exp(n^2\phi_1^2)} \right] \tag{96}
$$
$$
[\delta + (1-\delta)\pi r]
$$

and,

$$
\sqrt{\pi}\left\{ \delta\frac{h_S}{T_S}\frac{\Gamma_S(\vec{r} = \vec{S}_S)}{v_S} + (1-\delta)\frac{\Delta H}{v_L - v_S} \right\}\phi_1 a_S
$$
$$
= \left[k_{SL}\frac{n(T_{Liq} - T_{Sol})}{[\mathrm{erf}(\phi_2) - \mathrm{erf}(n\phi_1)]\exp(n^2\phi_1^2)} - k_S\frac{(T_{Sol} - T_0)}{[M + \mathrm{erf}(\phi_1)]\exp(\phi_1^2)} \right] \tag{97}
$$
$$
[(1-\delta) + \delta\pi r]
$$

In the case of solidification, $\delta = 0$, and the interface is a function of r, then the liquidus interface is a nucleation and growth site and the latent heat integration

occurs at the eutectic interface. For fusion, $\delta = 1$, the eutectic is a nucleation and growth site and liquidus is a latent heat integration isotherm.

$$\sqrt{\pi}\left\{\delta\frac{\Delta H}{v_L - v_S} + (1-\delta)\frac{h_L}{T_L}\frac{\Gamma_L(r = S_L)}{v_L}\right\}\phi_2 a_L$$

$$= \left[k_L\frac{m(T_P - T_{Liq})}{[1 - \operatorname{erf}(m\phi_2)]\exp\left(m^2\phi_2^2\right)} - k_{SL}\frac{(T_{Liq} - T_{Sol})}{[\operatorname{erf}(\phi_2) - \operatorname{erf}(n\phi_1)]\exp(n^2\phi_1^2)}\right]$$

$$[\delta + (1-\delta)\pi r]$$

(98)

and,

$$\sqrt{\pi}\left\{\delta\frac{h_S}{T_S}\frac{\Gamma_S(\vec{r} = \vec{S}_S)}{v_S} + (1-\delta)\frac{\Delta H}{v_L - v_S}\right\}\phi_1 a_S$$

$$= \left[k_{SL}\frac{n(T_{Liq} - T_{Sol})}{[\operatorname{erf}(\phi_2) - \operatorname{erf}(n\phi_1)]\exp(n^2\phi_1^2)} - k_S\frac{(T_{Sol} - T_0)}{[M + \operatorname{erf}(\phi_1)]\exp(\phi_1^2)}\right]$$

$$[(1-\delta)\pi r + \delta]$$

(99)

The Gibbs–Thomson coefficient, surface energy, surface tension, and nucleation radius for the liquidus and solidus isotherm positions are calculated from the microscopic scale and will be discussed in detail in the coming sections.

2.4.7 Determination of the Virtual Pre-existing Adjuncts to Mold (S_0, L_0 and E_0)

In the real system, the Newtonian resistance at the metal/mould interface is represented by the heat transfer coefficient h_i, which must be determined for each experiment. In the virtual system, a portion of the Newtonian thermal resistance is exchanged by an additional layer of solid, and it must be related to the heat transfer coefficient h_i. As both systems are equivalent, the same thermal behavior is expected. The real and virtual systems can be related to each other at the beginning of the solidification process. The heat fluxes at the mould for both systems must be the same. According to the real and virtual system, the following set of equations can be determined as a function of the total thermal resistance, i.e.,

$$h_S(T_{Sol} - T_i) = k_S\left(\frac{dT_S}{dx'}\right)_{x'=S_0}$$

(100)

where h_S is the Newtonian heat transfer coefficient at the metal/mould interface. The temperature T_i can be eliminated from Eq. 100 by comparing the thermal resistances, as shown in Fig. 2 as

$$h_g\left(T_{Liq} - T_0\right) = h_M\left(T_i - T_0\right) = h_S\left(T_{Sol} - T_i\right) = h_{SL}\left(T_{Liq} - T_{Sol}\right) \tag{101}$$

By applying $x' = S_0$ in $S'_S = S_0$ in Eq. 89 gives

$$\left.\left(\frac{\partial T_S}{\partial x'}\right)\right|_{x'=S_0} = \frac{2}{\sqrt{\pi}} \frac{\phi_1}{S_0} \frac{\left(T_{Sol} - T_0\right)}{M + erf\left(\phi_1\right)} \exp\left[-\left(\phi_1\right)^2\right] \tag{102}$$

By substituting Eqs. 101 and 102 into Eq. 100), the following relation is obtained:

$$S_0 = \frac{2}{\sqrt{\pi}} \frac{\phi_1}{\left(T_{Liq} - T_0\right)} \frac{k_S\left(T_{Sol} - T_0\right)}{\left[M + erf\left(\phi_1\right)\right]\exp\left(\phi_1\right)^2 h_g} \tag{103}$$

The pre-existing adjunct L_0 is related to S_0 from the boundary conditions Eqs. 44 and 45 and Eq. 95,

$$S'_S = nS'_L \frac{\phi_1}{\phi_2} \tag{104}$$

For $t' = t_0$, and considering $S'_S = S_0$ and $S'_L = L_0$ and substituting into Eq. 104 provides the following relationship:

$$S_0 = nL_0 \frac{\phi_1}{\phi_2} \tag{105}$$

The energy balance, at the beginning of solidification ($t = 0$) in the real coordinate system metal/mould interface, demands the following translation to the virtual system, $t' = t_0$ and $x' = -E_0$. In this case,

$$h_M\left(T_i - T_0\right) = k_M\left(\frac{dT_M}{dx'}\right)_{x'=-E_0} \tag{106}$$

Considering $x' = -E_0$ in $S'_S = L_0$ the thermal gradient can be evaluated

$$\left.\left(\frac{\partial T_M}{\partial x'}\right)\right|_{x'=-E_0} = \frac{2}{\sqrt{\pi}} \frac{N\phi_1}{L_0}\left(T_i - T_0\right)\exp\left[-\left(N\phi_1 \frac{E_0}{L_0}\right)^2\right] \tag{107}$$

By substituting Eq. 107 into Eq. 106, the following E_0 correlation can be obtained:

$$E_0 = \frac{L_0}{N\phi_1}\sqrt{\ln\frac{k_M}{h_M}\frac{2}{\sqrt{\pi}}\frac{N\phi_1}{L_0}} \tag{108}$$

Now, the heat transfer coefficient h_M at the mould must be expressed in terms of the global heat transfer h_g, and by applying Eq. 75 to eliminate T_i. In this case,

$$h_M = h_g \frac{(T_{Liq} - T_0)}{(T_{Sol} - T_0)} \frac{[M + erf(\phi_1)]}{M} \tag{109}$$

and, by substituting Eq. 109 and the product $N.M = \frac{k_S}{k_M}$ in Eq. 108, E_0 can be written as follows

$$E_0 = \frac{L_0}{N\phi_1} \sqrt{\ln \frac{2k_S\phi_1(T_{Sol} - T_0)}{\sqrt{\pi}(T_{Liq} - T_0)[M + erf(\phi_1)]h_g L_0}} \tag{110}$$

and, by introducing Eqs. 105 into 110, the final equation for E_0 is given by

$$E_0 = \frac{S_0}{N} \tag{111}$$

2.4.8 Expressions for the Solidification Time (*t*) and Velocity of the Solidification Front (*v*)

The solidification kinetics were handled previously by the relationship between the time in the virtual and in the real systems, by considering either that the kinetics represented by the pre-existing virtual adjunct is not the same as that expected for the liquid and solid metal domains, as no latent heat release is expected from the virtual layer. No energy barrier implies faster kinetics for heat conduction in the virtual adjunct domain. The similarity variables ϕ_1 and ϕ_2 can be obtained employing interface equations Eqs. 49 and 50 by considering a parabolic relationship between space and time, providing

$$\phi_1 = \frac{S'_S}{2\sqrt{a_S t'}} \tag{112}$$

and,

$$\phi_2 = \frac{S'_L}{2\sqrt{a_L t'}} \tag{113}$$

By rearranging Eqs. 112 and 113 for t' gives

$$t' = \frac{S'^2_S}{4a_S \phi_1^2} \tag{114}$$

and,

$$t' = \frac{S'^2_L}{4a_L \phi_2^2} \tag{115}$$

By setting $t = 0$, implies $S_S = S_L = 0$, according to Eqs. 33–36, which assumes

$$S'_S = S_S + L_0 \text{ and } S'_L = S_L + L_0 \text{ and } t' = t + t0 \tag{116}$$

By applying $S_S' = S_0$ and $t' = t_0$ into Eq. 114:

$$t_0 = \frac{S_0^2}{4a_S\phi_1^2} \tag{117}$$

By substituting Eqs. 35, 36, 116 and 117, into Eqs. 114 and 115, the following relationships for the times of displacement of solidus (t_S) and liquidus (t_L) isotherms are obtained:

for solidus

$$t_S + t_0 = t_S + \frac{S_0^2}{4a_S\phi_1^2} = \frac{(S_S^2 + 2S_S L_0 + L_0^2)}{4a_S\phi_1^2} + \frac{S_0^2}{4a_S\phi_1^2} \tag{118}$$

and for liquidus

$$t_L + t_0 = t_L + \frac{S_0^2}{4a_L\phi_2^2} = \frac{(S_L^2 + 2S_L L_0)}{4a_L\phi_2^2} + \frac{S_0^2}{4a_L\phi_2^2} \tag{119}$$

The time can be written as a function of S_0 and L_0, so that

$$t_S = \frac{S_S^2}{4a_S\phi_1^2} + \frac{L_0 S_S}{2a_S\phi_1^2} + \frac{L_0^2 - S_0^2}{4a_S\phi_1^2} = \alpha_S S_S^2 + \beta_S S_S + \delta \tag{120}$$

$$t_L = \frac{S_L^2}{4a_L\phi_2^2} + \frac{L_0 S_L}{2a_L\phi_2^2} = \alpha_L S_L^2 + \beta_L S_L \tag{121}$$

From Eqs. 110 and 111, S_0 and L_0 can be derived as

$$S_0 = \frac{2}{\sqrt{\pi}} \frac{\phi_1}{(T_{Liq} - T_0)} \frac{a_S c_{PS} d_S (T_{Sol} - T_0)}{[M + erf(\phi_1)]\exp(\phi_1)^2 h_g} \tag{122}$$

and,

$$L_0 = \frac{2}{\sqrt{\pi}} \frac{\phi_2}{(T_{Liq} - T_0)} \frac{a_S c_{PS} d_S (T_{Sol} - T_0)}{n[M + erf(\phi_1)]\exp(\phi_1)^2 h_g} \tag{123}$$

By substituting Eqs. 122 and 123 into Eqs. 120 and 121

$$t_S = \frac{S_S^2}{4a_S\phi_1^2} + \frac{c_{PS} d_S (T_{Sol} - T_0) S_S}{\sqrt{\pi}(T_{Liq} - T_0)\phi_1 [M + erf(\phi_1)]\exp(\phi_1)^2 h_g} + \frac{L_0^2 - S_0^2}{4a_S\phi_1^2} \tag{124}$$

and,

$$t_L = \frac{S_L^2}{4a_L \phi_2^2} + \frac{nc_{PS}d_S(T_{Sol} - T_0)S_L}{\sqrt{\pi}(T_{Liq} - T_0)\phi_2[M + erf(\phi_1)]\exp(\phi_1)^2 h_g} \quad (125)$$

By rewriting the time of the solidus and liquidus isotherms in terms of α_S, β_S, α_L and β_L, the following expressions are obtained:

$$t_S = \alpha_S S_S^2 + \beta_S S_S + \delta \quad (126)$$

and,

$$t_L = \alpha_L S_L^2 + \beta_L S_L \quad (127)$$

The deduced solidus and liquidus isotherm velocities, the reciprocal derivative of t_S and t_L, give

$$\frac{\partial S_S}{\partial t_S} = v_S = \frac{1}{2\alpha_S S_S + \beta_S} \quad (128)$$

and,

$$\frac{\partial S_L}{\partial t_L} = v_L = \frac{1}{2\alpha_L S_L + \beta_L} \quad (129)$$

3 Application of GTF at Liquidus and Solidus Isothermal Surfaces in the Microscopic Domain

The macroscopic energy balance of moving solidus and liquidus macroscopic interfaces demands the values of Gibbs–Thomson at liquidus, $\Gamma_L(r)$ Eq. 98 and solidus $\Gamma_S(r)$, Eq. 99, the sides of the microscopic moving interface are known beforehand to calculate similarity roots ϕ_1 and ϕ_2. By applying Eq. 1 into Eqs. 6 and 7 and by assuming spherical or any suitable shape (for ice, a hexagonal prism or cylindric can be assumed depending on concentration, temperature, volume and pressure gradients) for the surface area of the nucleus $A(\vec{r})$, as can be observed in Eqs. 1 and Eq. 23, which depends on temperature, volume, pressure and concentration gradients, isotherm velocity and cooling rate,

$$\frac{\left(\frac{r}{r_{Eq}}\right)^{\frac{\gamma_0}{2}} - s(r)}{A(r)(\Delta S_V - \Delta S_{surf})} = \frac{dT}{dr}\hat{e}_r \cdot \hat{n} = \left[\sum_{j=1}^{n-1}\left(\frac{\partial T}{\partial C_{L,j}}\right)_j \frac{\partial C_{L,j}}{\partial r}\hat{e}_r + \frac{\partial T}{\partial V}\frac{\partial V}{\partial r}\hat{e}_r + \frac{\partial T}{\partial P}\frac{\partial P}{\partial r}\hat{e}_r + \frac{\partial \widetilde{T}}{\partial r}\hat{e}_r\right] \cdot \hat{n} \quad (130)$$

In the absence of mechanical or electromagnetic vibration or agitation, the term $\frac{\partial T}{\partial P}\frac{\partial P}{\partial r}$ and $\frac{\partial T}{\partial V}\frac{\partial V}{\partial r}$ can be neglected, which provides

$$\frac{\frac{\gamma_0}{\left(\frac{r}{r_{Eq}}\right)^2} - s(r)}{A(r)\left(\Delta S_V - \Delta S_{surf}\right)} = \frac{dT}{dr}\widehat{e}_r \cdot \widehat{n} = \left[\sum_{j=1}^{n-1}\left(\frac{\partial T}{\partial C_{L,j}}\right)_j \frac{\partial C_{L,j}}{\partial r}\widehat{e}_r + \frac{\partial \widetilde{T}}{\partial r}\widehat{e}_r\right] \cdot \widehat{n} \tag{131}$$

The temperature and concentration gradients will be applied for the determination of surface energy, surface stress, nucleation radius and Gibbs–Thomson coefficients, which are necessary to determine the evolution of the macroscopic solidus and liquidus interfaces. Neglecting the pressure and volume gradients, considering a spherical nucleus of radius of r, and assuming $A(r) = 4\pi r^2$, provides the following expression for the nucleation radius at the liquidus temperature:

$$\frac{\frac{\gamma_0}{\left(\frac{r}{r_{Eq}}\right)^2} - s(r)}{4\pi r^2\left(\frac{\Delta H}{T_{Li}} - \frac{1}{\Delta T}\frac{\partial \gamma_{SL}}{\vec{\partial r}}\right)} = \left[\sum_{j=1}^{n-1}\left(\frac{\partial T}{\partial C_{L,j}}\right)_j \frac{\partial C_{L,j}}{\partial r}\widehat{e}_r + \frac{\partial \widetilde{T}}{\partial r}\widehat{e}_r\right] \cdot \widehat{n} \tag{132}$$

For the solidus side of the microscopic transformation moving interface,

$$\frac{\frac{\gamma_0}{\left(\frac{r}{r_{Eq}}\right)^2} - s(r)}{4\pi r^2\left(\frac{\Delta H}{T_{Si}} - \frac{1}{\Delta T}\frac{\partial \gamma_{SL}}{\vec{\partial r}}\right)} = \left[\sum_{j=1}^{n-1}\left(\frac{\partial T}{\partial C_{S,j}}\right)_j \frac{\partial C_{S,j}}{\partial r}\widehat{e}_r + \frac{\partial \widetilde{T}}{\partial r}\widehat{e}_r\right] \cdot \widehat{n} \tag{133}$$

Recently, Jahkar et al. [74] derived a similarity solution for solidification of undercooled binary alloys, including shrinkage-induced flow, in which the thermophysical properties are assumed to be constants within a phase but discontinuous between the solid and liquid phases, and temperature and concentration fields are coupled through the Lewis number. The solution derived by the authors encompassed only the solution for the liquid phase gradient, but in the present case, solid and liquid phase gradients are necessary. Problems arise concerning the stability of analytical solutions when concentration and temperature fields are coupled, according to Voller [13] and Swaminathan and Voller [66], and the only critical change of variable is given by Eq. 133

$$T^* = \widetilde{T} - \widetilde{T}_F - \sum_{j=1}^{n-1}\frac{\partial T}{\partial C_i}C_{o,j} \tag{134}$$

$$C^* = \frac{C}{C_0} \tag{135}$$

$$Le_S = \frac{a_S}{D_S} \tag{136}$$

$$Le_L = \frac{a_L}{D_L} \tag{137}$$

$$R = \frac{d_S}{d_L} \tag{138}$$

For the solid phase, $0 < x' < S'(t')$

$$\widetilde{T}_S^* = \widetilde{T}_0^* + \frac{\left(\widetilde{T}_{Si}^* - \widetilde{T}_0^*\right)}{M + \mathrm{erf}(\phi)} \left\{ M + \mathrm{erf}\left[\phi \frac{x + S_0}{S + S_0}\right] \right\}, \tag{139}$$

$$C_{S,j}^* = kC_{0,j}^* + \frac{\left(C_{Si,j}^* - k_j C_{0,j}^*\right)}{\mathrm{erf}\left[\phi\sqrt{Le_{S,j}}\right]} \mathrm{erf}\left[\phi\sqrt{Le_{S,j}}\frac{x + S_0}{S + S_0}\right] \tag{140}$$

For the liquid phase, $s'(t') < x' < +\infty$

$$\widetilde{T}_L^* = \widetilde{T}_{Li}^* - \frac{\left(\widetilde{T}_{Li}^* - \widetilde{T}_{Si}^*\right)}{1 - \mathrm{erf}(n\phi - n\phi(R-1))} \left\{ 1 - \mathrm{erf}\left[n\phi\frac{x + S_0}{S + S_0} - n\phi(R-1)\right] \right\} \tag{141}$$

$$C_{L,j}^* = C_{Li,j}^* - \frac{\left(C_{Li,j}^* - C_{Si,j}^*\right)}{1 - \mathrm{erf}\left[n\phi\sqrt{Le_L} - n\phi\sqrt{Le_L}(R-1)\right]} \left\{ 1 - \mathrm{erf}\left[n\phi\sqrt{Le_L}\frac{x + S_0}{S + S_0} - n\phi\sqrt{Le_{L,j}}(R-1)\right] \right\} \tag{142}$$

and the interface temperatures T_{Li}^* and T_{Si}^*, and concentrations C_{Li}^* and $C_{Si,j}^*$ can be derived as

$$\frac{d_S L}{R} \frac{dS'}{dt'} = k_S \left.\frac{\partial \widetilde{T}_S^*}{\partial x'}\right|_{x'=S'-} - k_L \left.\frac{\partial \widetilde{T}_L^*}{\partial x'}\right|_{x'=S'+} \tag{143}$$

$$\frac{\left(C_{Li,j}^* - C_{Si,j}^*\right)}{R} \frac{dS'}{dt'} = D_{S,j} \left.\frac{\partial C_{S,j}^*}{\partial x'}\right|_{x'=S'-} - D_{L,j} \left.\frac{\partial C_{L,j}^*}{\partial x'}\right|_{x'=S'+} \tag{144}$$

By deriving Eqs. 139–142 with respect to x' at the interface $x' = S'$,

$$\left.\frac{\partial \widetilde{T}_L^*}{\partial x'}\right|_{x'=S'+} = \frac{2n\phi\left(\widetilde{T}_{Li}^* - \widetilde{T}_{Si}^*\right)}{\sqrt{\pi}\{1 - \mathrm{erf}[n\phi - n\phi(R-1)]\}S'} e^{-[n\phi - n\phi(R-1)]^2} \tag{145}$$

$$\left.\frac{\partial C_{L,j}^*}{\partial x'}\right|_{x'=S'+} = \frac{2n\phi\sqrt{Le_{L,j}}\left(C_{L,j}^* - C_{S,j}^*\right)}{\sqrt{\pi}\left\{1 - \mathrm{erf}\left[n\phi\sqrt{Le_{L,j}} - n\phi\sqrt{Le_{L,j}}(R-1)\right]\right\}S'}e^{-\left[n\phi\sqrt{Le_{L,j}} - n\phi\sqrt{Le_{L,j}}(R-1)\right]^2}$$

(146)

$$\left.\frac{\partial \widetilde{T}_S^*}{\partial x'}\right|_{x'=S'-} = \frac{2\phi\left(\widetilde{T}_{Si}^* - \widetilde{T}_0^*\right)}{\sqrt{\pi}\{M + \mathrm{erf}(\phi)\}S'}e^{-[\phi]^2}$$

(147)

$$\left.\frac{\partial C_{S,j}^*}{\partial x'}\right|_{x'=S'-} = \frac{2\phi\sqrt{Le_{S,j}}\left(C_{L,j}^* - k_j C_{o,j}^*\right)}{\sqrt{\pi}\left\{\mathrm{erf}\left[\phi\sqrt{Le_{S,j}}\right]\right\}S'}e^{-\left[\phi\sqrt{Le_{S,j}}\right]^2}$$

(148)

To derive the interface temperature, T_{Si}^* the liquidus interface temperature is defined as a function of the temperature-concentration slope for each solute j, $m_{S,j} = \frac{\partial \widetilde{T}_S^*}{\partial C_{o,j}^*}$, as follows:

$$\widetilde{T}_{Li}^* = \widetilde{T}_F^* - \sum_{j=1}^{n-1}\frac{\partial \widetilde{T}^*}{\partial C_j^*}C_{o,j}^* = \widetilde{T}_F^* - \sum_{j=1}^{n-1}m_{L,j}C_{o,j}^*$$

(149)

since

$$C_{SV}^* + \sum_{j=1}^{n-1}C_{o,j}^* = 1$$

(150)

The interface temperature T_{Si}^* can be written as

$$\widetilde{T}_{Li}^* = \frac{\dfrac{\left(\widetilde{T}_{Si}^* - \widetilde{T}_0^*\right)}{[M + \mathrm{erf}(\phi)]e^{\phi^2}} + \dfrac{m\widetilde{T}_{Si}^*}{[1 - \mathrm{erf}(n\phi - n\phi(R-1))]e^{(n\phi - n\phi(R-1))^2}} - \dfrac{\sqrt{\pi}L\phi}{RC_{Ps}}}{\dfrac{m}{[1 - \mathrm{erf}(n\phi - n\phi(R-1))]e^{(n\phi - n\phi(R-1))^2}}}$$

(151)

and $C_{L,i}^*$

$$C_{L,j}^* = \frac{\dfrac{C_{0,j}^*}{\mathrm{erf}\left(\phi\sqrt{Le_{S,j}}\right)e^{(\phi)^2}}}{\dfrac{1}{\mathrm{erf}\left(\phi\sqrt{Le_{S,j}}\right)e^{(\phi\sqrt{Le_{S,j}})^2}} - \dfrac{D_{L,j}}{D_{S,j}}\dfrac{n}{\left[1 - \mathrm{erf}\left(n\phi\sqrt{Le_{L,j}} - n\phi\sqrt{Le_{L,j}}(R-1)\right)\right]e^{\left(n\phi\sqrt{Le_{L,j}} - n\phi\sqrt{Le_{L,j}}(R-1)\right)^2}} - \dfrac{\sqrt{\pi}L\phi\sqrt{Le_{S,j}}}{R}}$$

(152)

The equilibrium equation is expressed as a function of liquidus and solidus temperatures,

$$\widetilde{T}_F^* = \widetilde{T}_{Li}^* + \sum_{j=1}^{n-1}m_{L,j}C_{Li,j}^*$$

(153)

Then, Eq. 152 permits the similarity root ϕ to be calculated.

$$\widetilde{T}_F^* - \widetilde{T}_{Li}^* - \sum_{j=1}^{n-1} m_{L,j} C_{Li,j}^* = 0 \tag{154}$$

The temperature and concentration gradients of a semi-infinite slab will be applied to provide the nucleation radius at the liquidus and solidus sides of the microscopic moving transformation interface, Eqs. 144–147, by substituting them into Eqs. 132 and 133 at any position $S' = S + S_0$, and $S_0 = \frac{\beta}{2\alpha}$ based on the solidus and liquidus sides at the moving microscopic interface.

$$
\frac{\frac{\gamma_0}{\left(\frac{r}{r_{Eq}}\right)^2} - s(r)}{4\pi r^2 \left(\frac{\Delta H}{T_{Li}} - \frac{1}{\Delta T} \frac{\partial \gamma_{SL}}{\partial r}\right)}
$$

$$
= \left\{ \sum_{j=1}^{n-1} \frac{\partial T_L}{\partial C_{L,j}} \left[\frac{2n\phi \sqrt{Le_{L,j}} \left(C_{Li,j}^* - C_{Si,j}^*\right)}{\sqrt{\pi} \left\{1 - \mathrm{erf}\left[n\phi\sqrt{Le_{L,j}} - n\phi\sqrt{Le_{L,j}}(R-1)\right]\right\} \left(\frac{2\alpha S + \beta}{2\alpha}\right)} e^{-\left[n\phi\sqrt{Le_{L,j}} - n\phi\sqrt{Le_{L,j}}(R-1)\right]^2} \right] \right.
$$

$$
\left. + \frac{2n\phi\left(\widetilde{T}_{Li}^* - \widetilde{T}_{Si}^*\right)}{\sqrt{\pi}\{1 - \mathrm{erf}[n\phi - n\phi(R-1)]\}\left(\frac{2\alpha S + \beta}{2\alpha}\right)} e^{-[n\phi - n\phi(R-1)]^2} \right\} \widehat{e}_r \cdot \widehat{n}
\tag{155}
$$

$$
\frac{\frac{\gamma_0}{\left(\frac{r}{r_{Eq}}\right)^2} - s(r)}{4\pi r^2 \left(\frac{\Delta H}{T_{Si}} - \frac{1}{\Delta T} \frac{\partial \gamma_{SL}}{\partial r}\right)}
$$

$$
= \left\{ \sum_{j=1}^{n-1} \frac{\partial T_S}{\partial C_{S,j}} \left[\frac{2\phi\sqrt{Le_{S,j}}\left(C_{Si,j} - k_j C_{o,j}^*\right)}{\sqrt{\pi}\{\mathrm{erf}\left[\phi\sqrt{Le_{S,j}}\right]\}\left(\frac{2\alpha S + \beta}{2\alpha}\right)} e^{-\left[\phi\sqrt{Le_{S,j}}\right]^2} \right] + \frac{2\phi\left(\widetilde{T}_{Si} - \widetilde{T}_0\right)}{\sqrt{\pi}\{M + \mathrm{erf}(\phi)\}\left(\frac{2\alpha S + \beta}{2\alpha}\right)} e^{-[\phi]^2} \right\} \widehat{e}_r \cdot \widehat{n}
\tag{156}
$$

The surface stress tensor s, considering an isotropic mean, can be determined by the Gurtin and Murdoch [70] approach for spheres,

$$s = \frac{2\sigma_0}{r(1 + \alpha)} \tag{157}$$

and,

$$\alpha = \frac{2[\sigma_0 + 2(\lambda_0 + \mu_0)]}{r(3\lambda + 2\mu)} \tag{158}$$

where the σ_0 is the surface tension and λ, λ_0, μ and μ_0 are the Lamé moduli. Equations 157 and 158 will be used for local integration to provide an analytical solution for the surface stress tensor s at the nucleating surface $A(r)$.

4 Results and Discussion

The analytical model derived to calculate local temperature/concentration gradients is a closed-form solution, and it is used to reckon analytically by Eqs. 154–157 the critical radius, surface energy, surface tension, surface stress, local Gibbs–Thomson, critical nucleation energy, and rate. Based on numerical simulations, both the macroscopic present proposition and Garcia's model are dependent on the Biot and Fourier numbers, where only the Biot number was considered in the pre-existing virtual adjunct $h_g = f(S_0, L_0) = f(Biot, Fo, Biot^2 Fo)$. There is a relationship with the virtual adjunct for which the macroscopic solidification model is a closed-form solution.

The results and discussion section will be divided into microscopic and macroscopic solidification, since the temperature and species gradients must be provided for liquidus and solidus macroscopic interfaces, as both are dependent on the local nucleation conditions associated with the temperature, solute, volume, and pressure gradients captured by the Gibbs–Thomson coefficients, which are calculated at the microscopic transformation moving interface from the liquid and solid phase sides.

In Fig. 5 the temperature gradients are calculated at the solidus and liquidus sides of the microscopic interface for the very first solidified layer plotted against the global heat transfer coefficient h_g. As can be observed, according to Eq. 142 for higher values of h_g, the temperature gradient of the solid will increase faster than that of the liquid and the interface velocity will be controlled by the solid phase gradient.

In Fig. 6 the solute concentration is plotted against interface position $S = 4$ mm, considering the global heat transfer coefficient varying from $1 \ \mathrm{W \cdot m^{-2} \cdot K^{-1}}$ to $200 \mathrm{W \cdot m^{-2} \cdot K^{-1}}$. Assuming Lewis number for the solid, $Le_S = 10^3$, and for the liquid, $Le_L = 10^2$, a similar test was performed in Jakhar et al. [74]. As can be observed, for lower h_g the composition remains unchanged in the liquid region. For
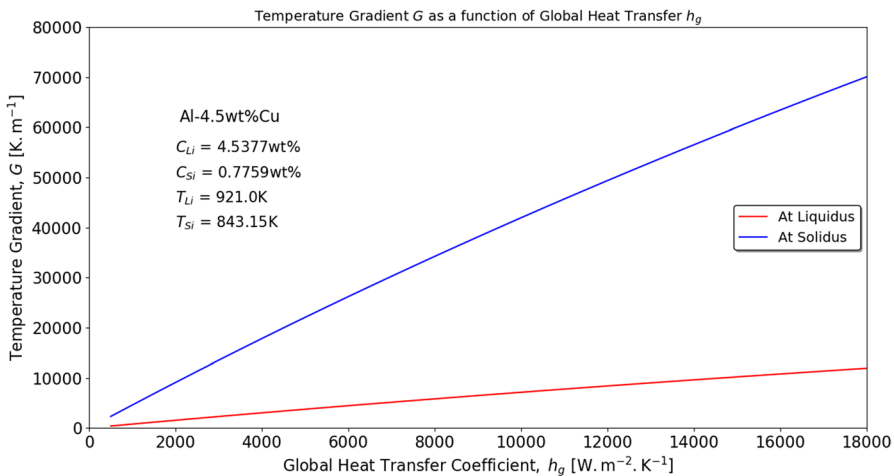
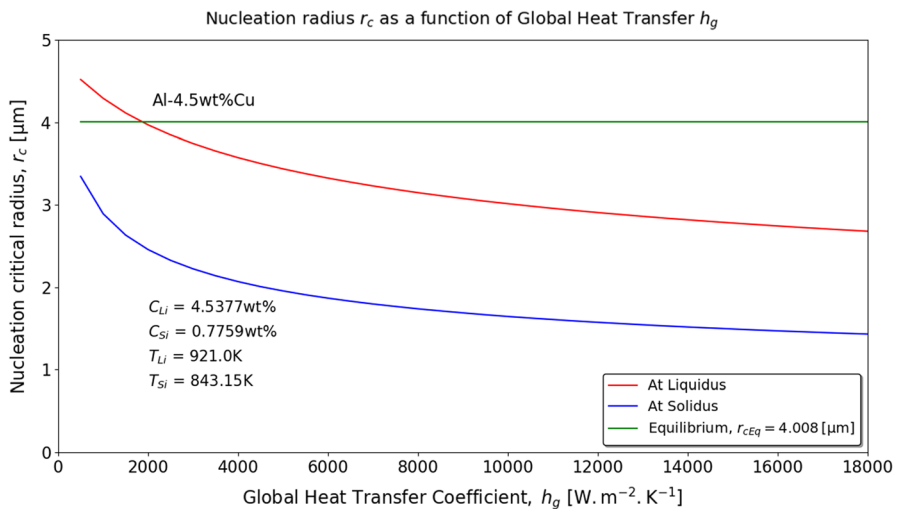**Fig. 5** Temperature gradients for positions close to the liquidus and solidus side of microscopic moving interface for the first solid layer
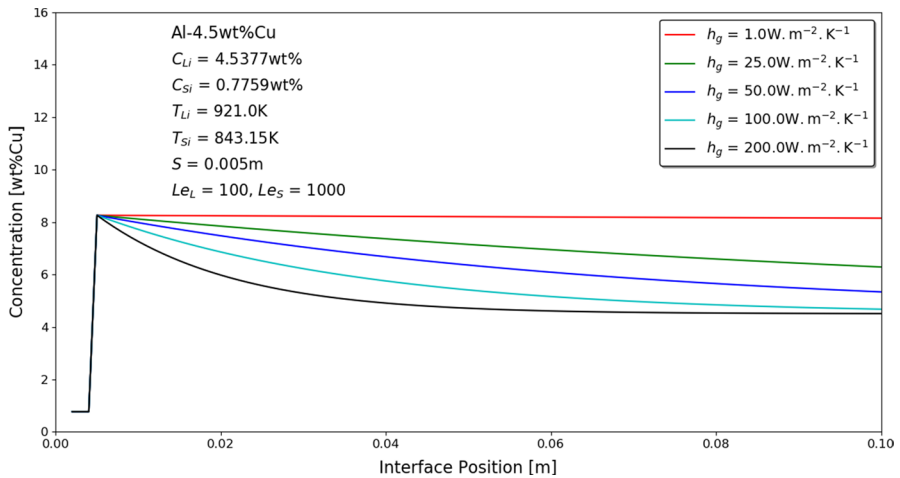
**Fig. 6** Concentration profiles as a function of microscopic phase-change interface position

higher h_g a continuous decrease in the concentration profile causes a decrease in the diffusion layer in the liquid, reaching the nominal alloy concentration closer to the interface.

Recently, Ferreira and Moreira [64] presented the transformation interfaces occurring during the solidification of Al-Xwt%Cu alloys for the composition range of Cu varying from pure Al to 33wt%Cu. The addition of Cu causes the single solidification interface to split into two, a liquidus and a solidus, until the solid phase Al-rich α_{Al} reaches its solubility limit at $C_S \sim 5.65$ wt% Cu, where a eutectic reaction

Fig. 7 Nucleation radius at positions close to the liquidus and solidus side of microscopic moving interface for the first solidified layer
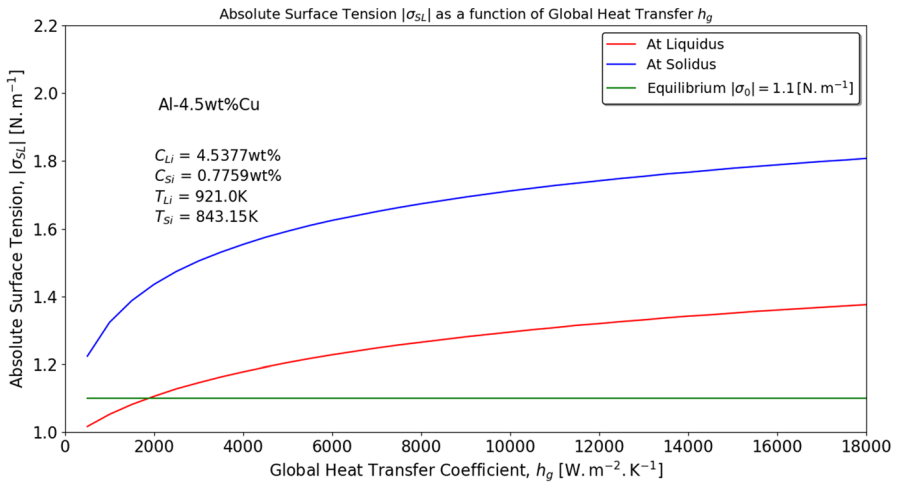
Fig. 8 Absolute surface tension at positions close to the liquidus and solidus side of the microscopic moving interface versus global heat transfer coefficient
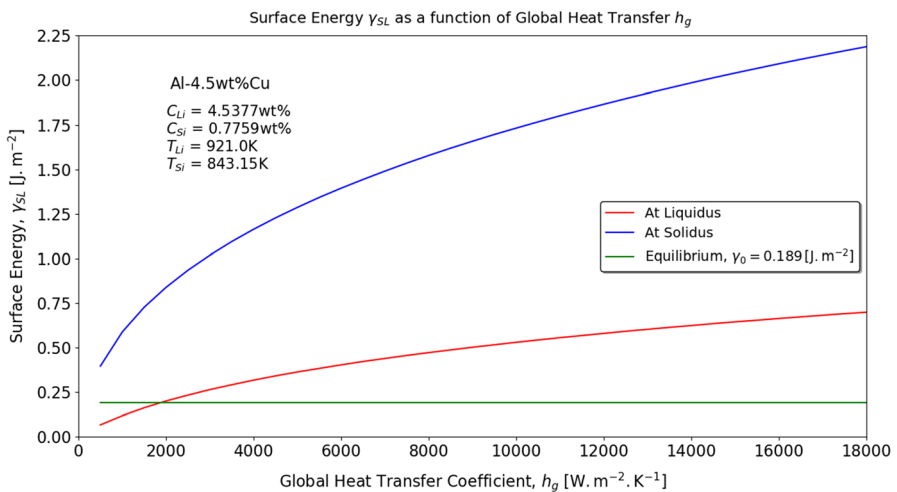
Fig. 9 Surface energy at positions close to the liquidus and solidus side of the microscopic moving interface versus global heat transfer coefficient

takes place. The eutectic solid interface remains until the liquidus isotherm reaches the eutectic concentration $C_L = C_{Eut}$, where a single eutectic interface governs the final instants of solidification. Considering only the liquidus and solidus isotherms, here for example, Fig. 7 shows the nucleation critical radius determined at both sides of the microscopic moving transformation interface, as the Gibbs–Thomson coefficient Γ at both the macroscopic liquidus and solidus fronts needs to be calculated to determine the similarity roots ϕ_1 and ϕ_2 by Eqs. 29 and 30. For the first solidified layer, considering the Al-4.5wt%Cu alloy as a function of the global heat transfer
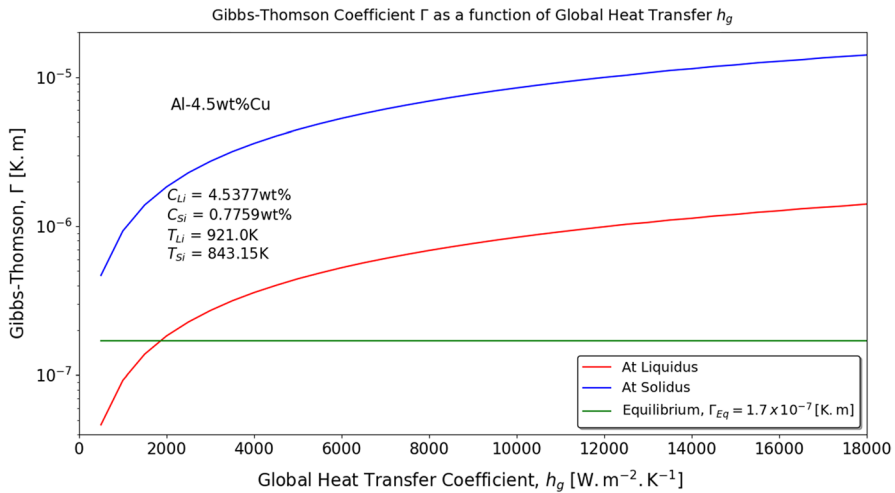
Fig. 10 Gibbs–Thomson coefficient close to the liquidus and solidus side of the microscopic moving interface as a function of the global heat transfer coefficient
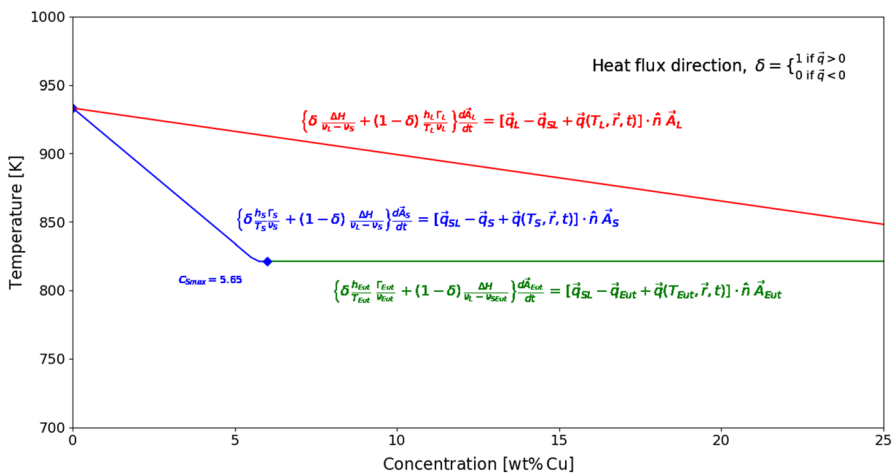
Fig. 11 Interface formulation for pure solvent and for liquidus and solidus interface versus solute content

coefficient h_g, the nucleation critical radius will decrease at the solidus and liquidus fronts compared with the equilibrium critical nucleation radius. At positions close to the solidus isotherm the lowest values of critical radius are found due to the higher thermal gradients.

Figures 8 and 9 present the surface tension and surface energy, respectively, for the first solidified layer of the Al-4.5wt%Cu alloy as a function of the global heat transfer coefficient, h_G. At both sides of the microscopic transformation interface, at liquidus and solidus temperatures, both surface tension and surface energy increase
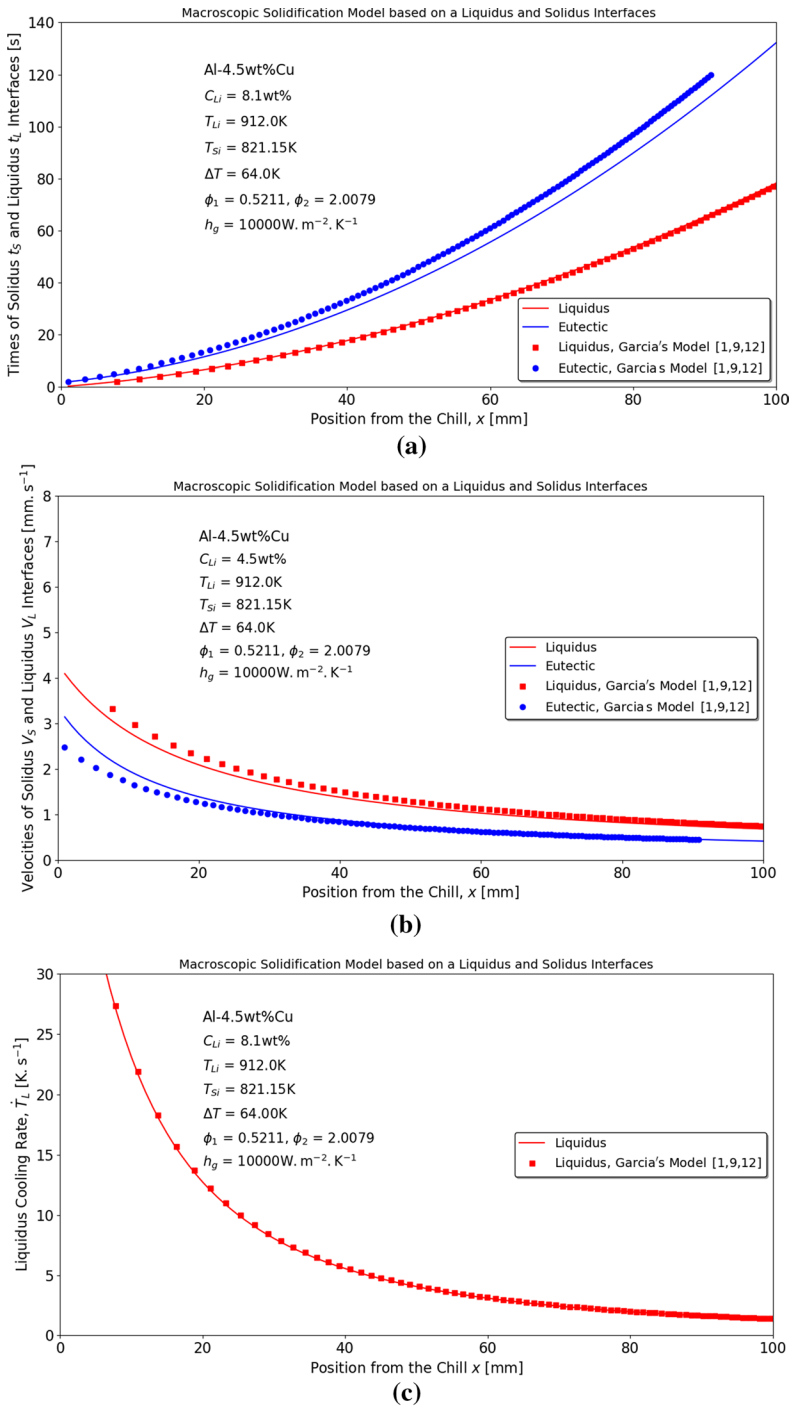
Fig. 12 Comparison between analytical models for Al-4.5wt%Cu, (a) Solidification times, (b) Isotherms velocities, and (c) liquidus cooling rates
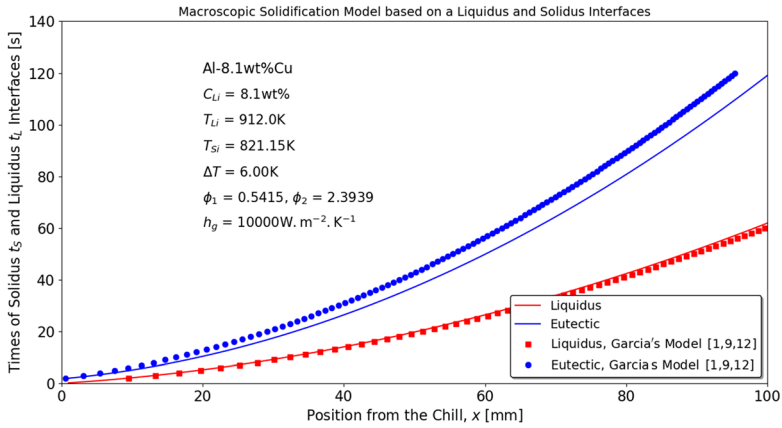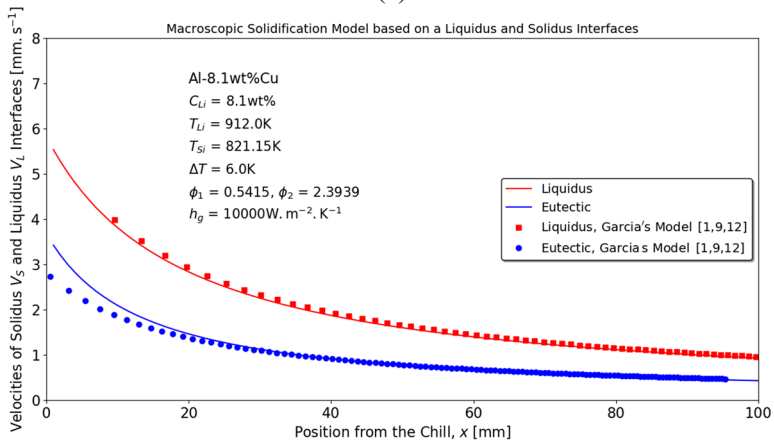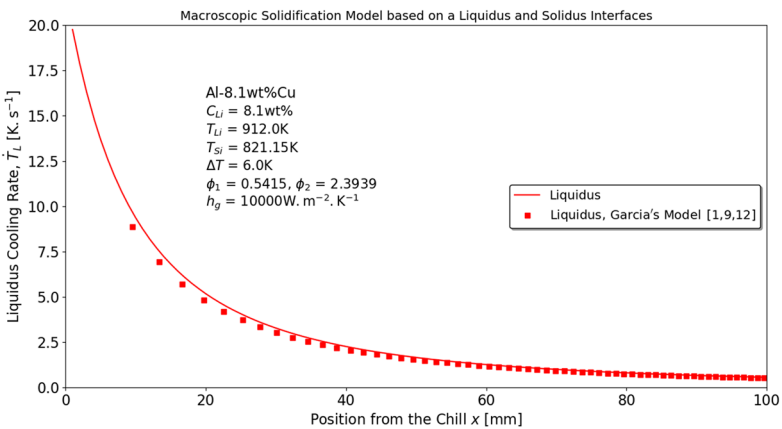
Fig. 13 Comparison between analytical models for Al-8.1wt%Cu, (a) Solidification times, (b) Isotherms velocities, and (c) liquidus cooling rates
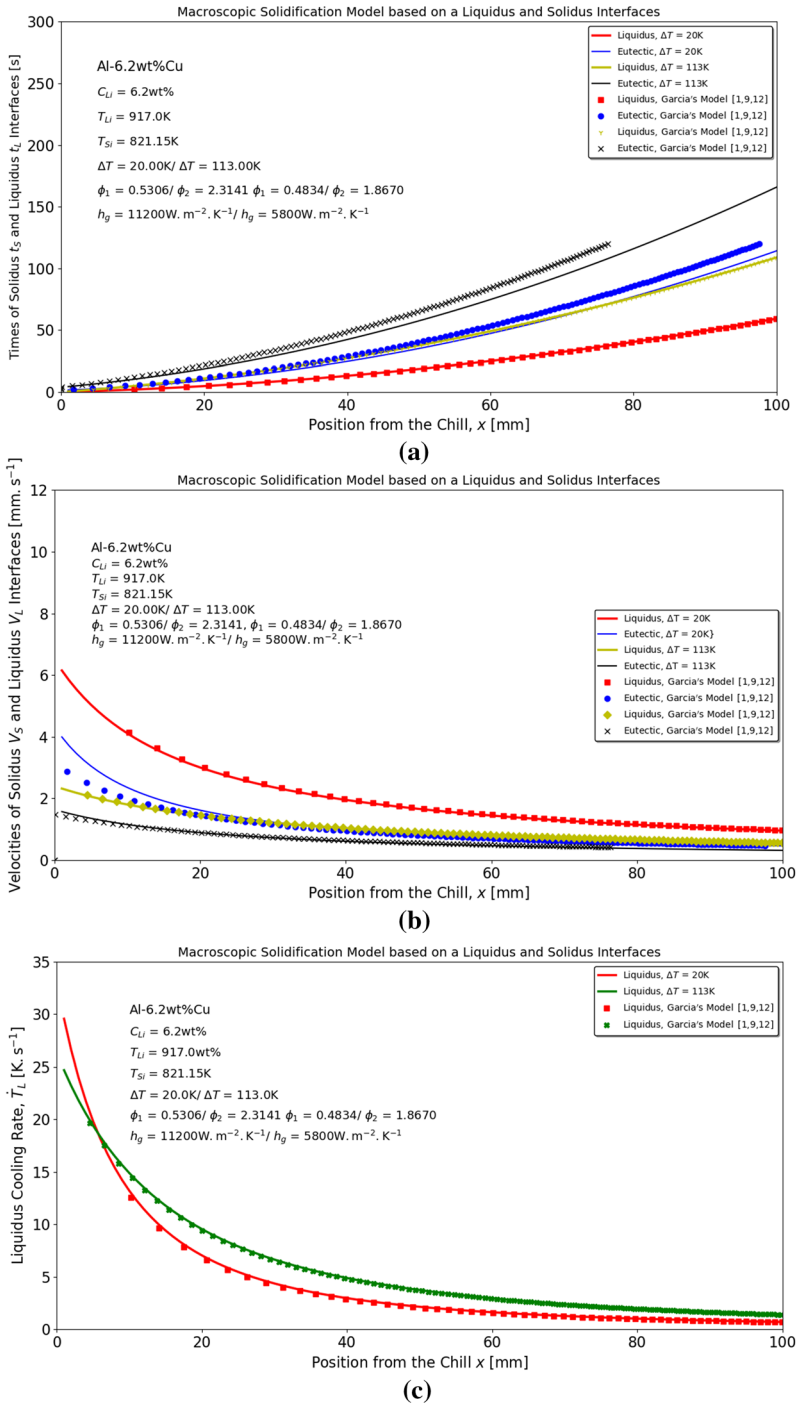
Fig. 14 Comparison between analytical models considering Al-6.2wt%Cu alloys subjected to different levels of melt superheat, for (a) Solidification times, (b) Isotherms velocities, and (c) liquidus cooling rates

with the increase in h_G. In the case of the liquidus isotherm, for $h_g > 2000 \mathrm{Wm^{-2}K^{-1}}$ both surface tension and surface energy are higher than those of equilibrium. The same behavior occurred for the critical radius. The surface energy is more sensitive to the kinetics than the surface tension. That is why Ferreira et al. [75] have noticed that the surface energy reaches similar values when the kinetics are considered (120 to 1540 K.min^{-1}) due to the surface area deformation [17].

Figure 10 shows the Gibbs–Thomson coefficients calculated at both sides of the microscopic moving transformation interface relative to the liquidus Γ_L and solidus Γ_S isotherms for the first solidified layer as a function of the global heat transfer coefficient. These coefficients are related to the nucleation resistance of liquidus $\frac{h_L}{T_L} \frac{\Gamma_L(\vec{r})}{v_L}$ and eutectic $-\frac{h_S}{T_S} \frac{\Gamma_S(\vec{r})}{v_S}$ on the moving interfaces depending on the heat flow direction under nucleation, which is related to the heat flux direction of the integration of latent heat, i.e., fusion or solidification as shown in Fig. 11.

The evaluation of the proposed multiscale model assumes that the Lamé moduli are the same for Cu compositions varying in the range from 4.5 wt% to 8.1 wt%. A microscopic multicomponent model was derived to calculate the liquidus and solidus thermal gradients necessary to compute the surface energy, surface tension, Gibbs–Thomson coefficient, local nucleation critical radius, energy and nucleation rate as a function of thermal gradients. The multiscale model is validated against the model proposed by Garcia [1] for the transient solidification of binary alloys. The macroscopic model developed is a multicomponent model, as it is coupled to the multicomponent microsegregation model. In the case of the proposed macroscopic model, velocities were considered from both interfaces, i.e., the proposed eutectic and liquidus. The alloy compositions chosen are Al-4.5 wt% Cu, Al-6.2 wt% Cu, and Al-8.1 wt% Cu, in Figs. 12, 13, and 14, respectively. In Fig. 12 good agreement is found for the liquidus position, velocity and cooling rate. In the case of eutectic times and velocities, a similar trend can be noticed for higher positions. In Fig. 13 a similar behavior can be observed. However, for low superheats, the agreement is improved. In the case of Fig. 14, again, excellent agreement can be noticed for the liquidus isotherm times, velocities and cooling rates for both low and high superheats. Considering the eutectic isotherm for the highest superheat $\Delta T = 113K$, the proposed model occurred for higher times when compared with Garcia's model [1]. On the other hand, for the isotherm growth rates, both models have a similar behavior.

5 Conclusions

In this paper, a multi-scalar analytical solution was proposed for the unsteady solidification of multicomponent alloys by solving the microscopic local temperature field and compositional fields and coupling the nucleation with local kinetics based on the Gibbs–Thomson-Ferreira-GTF equation [64], which was recently proposed [17]. Surface energy based on area creation and deformation formulation was solved for homogeneous and heterogeneous nucleation, critical radius, critical nucleation energy, and nucleation rate.

The derived model can predict the decrease in crystal regularity and the crystalline-glassy transition by considering the volumetric and surface entropy relationship in the present formulation of nucleation. An analytical solution for nucleation was proposed by considering the surface stress tensor, solidification shrinkage, and temperature and concentration coupled fields assuming that the analytical solution of a slab can be applied for the one-dimensional solidification/fusion problem, depending on δ. The microscopic and macroscopic models were applied to Al-Cu alloys, and the macroscopic model was plotted against a well-known analytical solution for transient solidification of binary alloys. A macroscopic multicomponent solidification model was derived and found to provide a similar solution to a well-known analytical model [1]. Numerical analysis has shown that the present macroscopic model provides an exact solution, and a set of dependencies of S_0 and L_0 virtual adjuncts on Fourier and Biot numbers need to be determined. The results of the model with the addition of interfaces were very similar to those calculated without the equations for the interfaces, which reiterates the robustness of the model previously deduced [1] and, at the same time, confirms the validity of the interface formulation.

Declarations

References

1. A. Garcia, *Solidificação: Fundamentos e Aplicações*, 2nd edn. (University of Campinas Publishing House, Campinas, 2007), pp.117–199
2. H.S. Carslaw, J.C. Jaeger, *Conduction of Heat in Solids*, 2nd edn. (Clarendon Press, Oxford, 1959), pp.282–296
3. A. Mori, K. Akari, Methods of analysis of the moving boundary-surface problem. Int. J. Chem. Eng. **16**, 734 (1976)
4. M.N. Ozisik, *Finite Difference Methods in Heat Transfer*, 1st edn. (CRC Press, Boca Raton, 1994), p.417
5. R.M. Furzeland, A survey of the formulation and solution of free and moving boundary (Stefan) problems, Brunel University Math. Report (1977)
6. A. Garcia, M. Prates, Metall. Trans. B (1978). https://doi.org/10.1007/BF02654420
7. A. Garcia, T.W. Clyne, M. Prates, Metall. Trans. B (1979). https://doi.org/10.1007/BF02653977

8. J. Lipton, A. Garcia, W. Heinemann, Arch. Eisenhüttenw. (1982). https://doi.org/10.1002/srin.198205182

9. D. Bouchard, J.S. Kirkaldy, Metall. Mater. Trans. A (1997). https://doi.org/10.1007/s11663-997-0039-x

10. M. Rappaz, W.J. Boettinger, Acta Mater. (1999). https://doi.org/10.1016/S1359-6454(99)00188-3

11. J.M.V. Quaresma, C.A. Santos, A. Garcia, Metall. Mater. Trans. A: Phys. Metall. Mater. Sci. (2000). https://doi.org/10.1007/s11661-000-0096-0

12. M. Rappaz, A. Jacot, W.J. Boettinger, Metall. Mater. Trans. A: Phys. Metall. Mater. Sci. (2003). https://doi.org/10.1007/s11661-003-0083-3

13. V.R. Voller, Trans. Indian Inst. Met. (2009). https://doi.org/10.1007/s12666-009-0042-9

14. A. Hamasaiid, M.S. Dargusch, T. Loulou, G. Dour, Int. J. Therm. Sci. (2011). https://doi.org/10.1016/j.ijthermalsci.2011.02.016

15. D.V. Alexandrov, A.A. Ivanov, I.V. Alexandrova, Philos. Trans. R. Soc. A (2018). https://doi.org/10.1098/rsta.2017.0217

16. I.L. Ferreira, A. Garcia, A.L.S. Moreira, Int. J. Math. Math. (2021). https://doi.org/10.1155/2021/6624287

17. I.L. Ferreira, Int. J. Thermophys. (2022). https://doi.org/10.1007/s10765-021-02956-0

18. I.L. Ferreira, A. Garcia, A.L.S. Moreira, J. Therm. Anal. Calorim. (2022). https://doi.org/10.1007/s10973-021-11153-y

19. J. Crank, in *Numerical Methods in Heat Transfer*. ed. by R.W. Lewis, K. Morgan, O.C. Zienkiewicsz (Wiley, New York, 1981), p.177

20. M. El-Bealy, Metall. Mater. Trans. B (2000). https://doi.org/10.1007/s11663-000-0052-9

21. L. Tan, N. Zabaras, J. Comput. Phys. (2007). https://doi.org/10.1016/j.jcp.2006.06.003

22. H. Hou, Y. Zhao, X. Niu, Trans. Nonferrous Met. Soc. China (2008). https://doi.org/10.1016/S1003-6326(10)60207-5

23. M.F. Zhu, T. Dai, S.Y. Lee, C. Hong, Comput. Math. Appl. (2008). https://doi.org/10.1016/j.camwa.2007.08.023

24. A.A. Ranjbar, A. Ghaderi, P. Dousti, M. Famouri, Int. J. Eng. **23**, 273 (2010)

25. A. Choudhury, K. Reuther, E. Wesner, A. August, B. Nestler, M. Rettenmayr, Comput. Mater. Sci. (2012). https://doi.org/10.1016/j.commatsci.2011.12.019

26. J. Li, Z. Wang, Y. Wang, J. Wang, Acta Mater. (2012). https://doi.org/10.1016/j.actamat.2011.11.037

27. M. Eshraghi, S.D. Felicelli, B. Jelinek, J. Cryst. Growth (2012). https://doi.org/10.1016/j.jcrysgro.2012.06.002

28. X. Zhang, J. Zhao, H. Jiang, M. Zhu, Acta Mater. (2012). https://doi.org/10.1016/j.actamat.2011.12.045

29. Y. Shi, Q. Xu, B. Liu, Trans. Nonferrous Met. Soc. China (2012). https://doi.org/10.1016/S1003-6326(11)61529-X

30. Z. Guo, J. Mi, P.S. Grant, IOP Conf. Ser.: Mater. Sci. Eng. (2012). https://doi.org/10.1088/1757-899X/33/1/012101

31. B. Jelinek, M. Eshraghi, S. Felicelli, J.F. Peters, Comput. Phys. Commun. (2014). https://doi.org/10.1016/j.cpc.2013.09.013

32. M. Paliwal, I.H. Jung, J. Cryst. Growth (2014). https://doi.org/10.1016/j.jcrysgro.2014.02.010

33. M. Zhu, D. Sun, S. Pan, Q. Zhang, D. Raabe, Model. Simul. Mater. Sci. Eng. (2014). https://doi.org/10.1088/0965-0393/22/3/034006

34. A. Viardin, M. Založnik, Y. Souhar, M. Apel, H. Combeau, Acta Mater. (2017). https://doi.org/10.1016/j.actamat.2016.10.004

35. A.M. Jokisaaria, P.W. Voorheesa, J.E. Guyerd, J.A. Warrend, O.G. Heinonen, Comput. Mater. Sci. (2018). https://doi.org/10.1016/j.commatsci.2018.03.015

36. B. Wu, A.L. Jiang, H. Lu, H.L. Zheng, X.L. Tian, Mater. Sci. Forum. (2018). https://doi.org/10.4028/www.scientific.net/MSF.913.212

37. C. Gu, C.D. Ridgeway, A.A. Luo, Metall. Mater. Trans. B (2019). https://doi.org/10.1007/s11663-018-1480-8

38. D. Montes de Oca Zapiain, J.A. Stewart, R. Dingreville, Comput. Mater. Sci. (2021). https://doi.org/10.1038/s41524-020-00471-8

39. D. Tourret, H. Liu, J. Lorca, Prog. Mater. Sci. (2022). https://doi.org/10.1016/j.pmatsci.2021.100810

40. K.D. Noubary, M. Kellner, B. Nestler, Materials (2022). https://doi.org/10.3390/ma15031160

41. V.P. Laxmipathy, F. Wang, M. Selzer, B. Nestler, Metals (2022). https://doi.org/10.3390/met12 030376

42. Y. Le Bouar, A. Finel, B. Appolaire, M. Cottura, Phase field models for modeling microstructures evolution in single crystal Ni-base super alloy, in *Nickel Base Single Crystals Across Length Scales*. ed. by G. Cailletaud, J. Cormier, G. Eggeler, V. Maurel, L. Nazé (Elsevier, Amsterdam, 2022), pp.379–399

43. L. Ceschini, I. Boromei, A. Morri, S. Seifeddine, I.L. Svensson, J. Mater. Process. Technol. (2009). https://doi.org/10.1016/j.jmatprotec.2009.05.030

44. M. Easton, C. Davidson, D. John, Metall. Mater. Trans. A: Phys. Metall. Mater. Sci. (2010). https://doi.org/10.1007/s11661-010-0183-9

45. D.B. Carvalho, E.C. Guimarães, A.L.S. Moreira, D.J. Moutinho, J.M. Dias-Filho, O.L. Rocha, Mater. Res. (2013). https://doi.org/10.1590/S1516-14392013005000072

46. V.A. Hosseini, S.G. Shabestari, R. Gholizadeh, Mater. Des. (2013). https://doi.org/10.1016/j.mat-des.2013.02.088

47. A.L.S. Moreira, O.F.L. Rocha, J.E. Spinelli, D.L.B. Carvalho, D.J.C. Moutinho, J.M.S. Dias Filho, Mater. Res. (2014). https://doi.org/10.1590/S1516-14392014005000015

48. J.D. Miller, T.M. Pollock, Acta Mater. (2014). https://doi.org/10.1016/j.actamat.2014.05.040

49. K.G. Prashanth, S. Scudino, H.J. Klauss, K.B. Surreddi, L. Löber, Z. Wang, A.K. Chaubey, U. Kühn, J. Eckert, Mater. Sci. Eng. A (2014). https://doi.org/10.1016/j.msea.2013.10.023

50. A.L.S. Moreira, A.S. Barros, I.A.B. Magno, F.A. Souza, C.A.M. Mota, M.A.P.S. Silva, O.F.L. Rocha, Met. Mater. Int. (2015). https://doi.org/10.1007/s12540-015-4499-2

51. E. Acer, E. Çadirli, H. Erol, M. Gündüz, Metall. Mater. Trans. A: Phys. Metall. Mater. Sci. (2016). https://doi.org/10.1007/s11661-016-3484-9

52. E. Karaköse, M. Yildiz, M. Keskin, Metall. Mater. Trans. B (2016). https://doi.org/10.1007/s11663-016-0678-x

53. E. Çadırlı, U. Büyük, S. Engin, H. Kaya, J. Alloys Compd. (2017). https://doi.org/10.1016/j.jallcom.2016.10.010

54. M. Riestra, E. Ghassemali, T. Bogdanoff, S. Seifeddine, Mater. Sci. Eng. A (2017). https://doi.org/10.1016/j.msea.2017.07.074

55. A. Medjahed, A. Henniche, M. Derradji, T. Yu, Y. Wang, R. Wu, L. Hou, J. Zhang, X. Li, M. Zhang, Mater. Sci. Eng. A (2018). https://doi.org/10.1016/j.msea.2018.01.118

56. Ü. Bayram, N. Maraşlı, Metall. Mater. Trans. B (2018). https://doi.org/10.1007/s11663-018-1404-7

57. X. Dong, S. Ji, J. Mater. Sci. (2018). https://doi.org/10.1007/s10853-018-2022-0

58. A. Barros, C. Cruz, A. Silva, N. Cheung, A. Garcia, O. Rocha, A. Moreira, Acta Metall. Sin-Engl. (2019). https://doi.org/10.1007/s40195-018-0852-z

59. A.P. Hekimoglu, M. Çalıs, G. Ayata, Met. Mater. Int. (2019). https://doi.org/10.1007/s12540-019-00429-6

60. T. Gu, B. Chen, C. Tan, J. Feng, Optics (2019). https://doi.org/10.1016/j.optlastec.2018.11.008

61. Y.Z. Li, N. Mangelinck-Noël, G. Zimmermann, L. Sturz, H. Nguyen-Thi, J. Alloys Compd. (2020). https://doi.org/10.1016/j.jallcom.2020.155458

62. S. Birinci, S. Basit, N. Marasli, J. Mater. Eng. Perform. (2022). https://doi.org/10.1007/s11665-021-06564-9

63. H. Li, G. Wang, Z. Qui, Z. Zheng, D. Zeng, Adv. Eng. Mater. (2022). https://doi.org/10.1002/adem.202200142

64. I.L. Ferreira, A.L.S. Moreira, *Designing Shape of Nucleus and Grain Coalescence during Alloy Solidification in 3d-ICOMAS Conference*. Verona (2022)

65. A. Karma, D. Tourret, Curr. Opin. Solid State (2016). https://doi.org/10.1016/j.cossms.2015.09.001

66. C.R. Swaminathan, V.R. Voller, Int. J. Mass Transf. (1997). https://doi.org/10.1016/S0017-9310(96)00329-8

67. J. Ni, C. Beckermann, Metall. Trans. B (1991). https://doi.org/10.1007/BF02651234

68. J. Crank, *Free and Moving Boundary Problems*, 1st edn. (Oxford University Press Inc., New York, 1996), pp.16–17

69. R. Shuttleworth, Proc. Phys. Soc. A (1950). https://doi.org/10.1088/0370-1298/63/5/302

70. M.E. Gurtin, A.I. Murdoch, Int. J. Solids Struct. (1978). https://doi.org/10.1016/0020-7683(78)90008-2

71. P. Müller, A. Saul, F. Leroy, Nanosci. Nanotechnol. (2014). https://doi.org/10.1088/2043-6262/5/1/013002

72. I.L. Ferreira, Int. J. Thermophys. (2021). https://doi.org/10.1007/s10765-021-02903-z

73. W. Di, L. Dezhi, W. Zhenyong, Comp. Sci. Info. Technol. (2015). https://doi.org/10.5121/csit.2015.51104
74. A. Jakhar, P. Rath, S.K. Mahapatra, Eng. Sci. Technol. (2016). https://doi.org/10.1016/j.jestch.2016.04.002
75. I.L. Ferreira, A.L.S. Moreira, J. Aviz, T.A. Costa, O.F.L. Rocha, A.S. Barros, A. Garcia, J. Manuf. Proc. (2018). https://doi.org/10.1016/j.jmapro.2018.08.010